In situ measurements of tropospheric volcanic plumes in Ecuador and Colombia during TC[4]

S. A. Carn,[1] K. D. Froyd,[2] B. E. Anderson,[3] P. Wennberg,[4] J. Crounse,[4] K. Spencer,[4] J. E. Dibb,[5] N. A. Krotkov,[6] E. V. Browell,[3] J. W. Hair,[3] G. Diskin,[3] G. Sachse,[3] and S. A. Vay[3]

[1] A NASA DC-8 research aircraft penetrated tropospheric gas and aerosol plumes sourced from active volcanoes in Ecuador and Colombia during the Tropical Composition, Cloud and Climate Coupling (TC[4]) mission in July–August 2007. The likely source volcanoes were Tungurahua (Ecuador) and Nevado del Huila (Colombia). The TC[4] data provide rare insight into the chemistry of volcanic plumes in the tropical troposphere and permit a comparison of SO_2 column amounts measured by the Ozone Monitoring Instrument (OMI) on the Aura satellite with in situ SO_2 measurements. Elevated concentrations of SO_2, sulfate aerosol, and particles were measured by DC-8 instrumentation in volcanic outflow at altitudes of 3–6 km. Estimated plume ages range from ~2 h at Huila to ~22–48 h downwind of Ecuador. The plumes contained sulfate-rich accumulation mode particles that were variably neutralized and often highly acidic. A significant fraction of supermicron volcanic ash was evident in one plume. In-plume O_3 concentrations were ~70%–80% of ambient levels downwind of Ecuador, but data are insufficient to ascribe this to O_3 depletion via reactive halogen chemistry. The TC[4] data record rapid cloud processing of the Huila volcanic plume involving aqueous-phase oxidation of SO_2 by H_2O_2, but overall the data suggest average in-plume SO_2 to sulfate conversion rates of ~1%–2% h^{-1}. SO_2 column amounts measured in the Tungurahua plume (~0.1–0.2 Dobson units) are commensurate with average SO_2 columns retrieved from OMI measurements in the volcanic outflow region in July 2007. The TC[4] data set provides further evidence of the impact of volcanic emissions on tropospheric acidity and oxidizing capacity.

1. Introduction

[2] Volcanoes are an important natural source of atmospheric particles, both primary (emitted to the atmosphere directly; e.g., volcanic ash derived from fragmented magma) and secondary (formed via gas-to-particle conversion, e.g., sulfate aerosol). The potentially global impact of stratospheric sulfate aerosol veils formed after injection of sulfur dioxide (SO_2) by explosive volcanic eruptions is well known [e.g., *Robock*, 2000]. However, tropospheric vol-

canic aerosols (see review by *Mather et al.* [2003a]) also affect climate and atmospheric radiation, both directly by increasing short-wave albedo, and indirectly by supplying cloud condensation nuclei (CCN) and affecting cloud microphysics and radiative properties [*Twomey*, 1974; *Jensen and Toon*, 1992; *Robock*, 2000; *Gassó*, 2008]. Furthermore, as sustained sources of acidic gases, aerosol precursors, and heavy metals, volcanic emissions in the lower troposphere and planetary boundary layer (PBL) can impact human health, the near-surface environment and even ocean productivity on local to regional scales [e.g., *Baxter et al.*, 1982; *Mannino et al.*, 1996; *Watson*, 1997; *Delmelle*, 2003; *Mather et al.*, 2003a; *Hansell and Oppenheimer*, 2004; *Longo et al.*, 2005; *Horwell and Baxter*, 2006; *Duggen et al.*, 2007; *Langmann et al.*, 2010]. On a time-averaged basis, data collected between the early 1970s and 1997 indicate that tropospheric SO_2 emissions from quiescent volcanic degassing and small eruptions surpass SO_2 loading in the upper troposphere and lower stratosphere (UTLS) from major explosive eruptions [e.g., *Andres and Kasgnoc*, 1998]. Although the magnitude of global anthropogenic SO_2 emissions greatly exceeds volcanic output, the

[1]Department of Geological and Mining Engineering and Sciences, Michigan Technological University, Houghton, Michigan, USA.
[2]NOAA Earth System Research Laboratory, Boulder, Colorado, USA.
[3]Science Directorate, NASA Langley Research Center, Hampton, Virginia, USA.
[4]Department of Geological and Planetary Sciences, California Institute of Technology, Pasadena, California, USA.
[5]Department of Earth Sciences, University of New Hampshire, Durham, New Hampshire, USA.
[6]Goddard Earth Sciences and Technology Center, University of Maryland Baltimore County, Baltimore, Maryland, USA.

former are typically released into the PBL, with correspondingly shorter lifetimes of emitted gases and aerosols (due largely to faster deposition in the PBL), whereas volcanic degassing occurs from vents at altitudes up to ~6 km above sea level. As a result, modeling suggests that 14%–36% of the global tropospheric sulfate burden may be volcanogenic [*Chin and Jacob*, 1996; *Graf et al.*, 1997].

[3] Assessment of the potential impact of volcanic emissions on climate, radiation, health and aviation requires detailed characterization of the chemical composition and particle size distribution (PSD) of the constituent gases and particles. Particle size and composition (which influences density and solubility) influence a particle's atmospheric lifetime and its viability as a CCN. Remote sensing techniques can be used to infer or measure SO_2 [e.g., *Carn et al.*, 2008], ash loading [e.g., *Wen and Rose*, 1994], sulfate aerosol abundance [e.g., *Yu and Rose*, 2000; *Karagulian et al.*, 2010], and some PSD information [*Mather et al.*, 2004a] in volcanic plumes, but the vertical sensitivity of such measurements is generally low. There are several important characteristics of volcanic emissions (e.g., size-resolved particle composition, vertical profiles of trace gases) that can only be elucidated through direct sampling.

[4] We report here one of the most comprehensive in situ data sets collected to date within volcanic plumes. The data were acquired during the NASA Tropical Composition, Cloud and Climate Coupling (TC⁴) experiment, based in San José, Costa Rica in July–August 2007 [*Toon et al.*, 2010] (http://www.espo.nasa.gov/tc4). Atmospheric sampling in the Intertropical Convergence Zone (ITCZ) during TC⁴ was focused on understanding the photochemical environment in the tropical troposphere, the interaction between chemical transport and convection, and the evaluation of retrievals from various spaceborne instruments. A large suite of long-lived tracers and reactive gases, along with particle size and composition data, were measured from the NASA DC-8 research aircraft (Table 1). The volcanic plume sampling in Ecuador and Colombia was opportunistic; guided by frequent observations of volcanic SO_2 degassing in the region by the Ozone Monitoring Instrument (OMI) since the launch of the Aura satellite in July 2004 [*Carn et al.*, 2008] (Figure 1). The TC⁴ campaign offered a chance to attempt validation of the OMI SO_2 measurements although, as we discuss below, issues with sampling time and low SO_2 levels mean that the principal merit of the TC⁴ data lies in the insight they provide into the composition of young and aged tropical volcanic plumes.

[5] The TC⁴ measurements are one of relatively few data sets derived from direct sampling of volcanic plumes in the tropical lower troposphere. Volcanic emissions have rarely been sampled at the ages encountered during TC⁴ (>30 h; section 4), offering rare insight into the composition of tropospheric volcanic plumes in the far field [see also *Oppenheimer et al.*, 2010]. An understanding of the composition of aged plumes, and hence their potential effects on atmospheric chemistry and climate, is crucial because of their extended atmospheric residence times.

[6] We provide here a selective summary of past efforts to sample volcanic plume gases and particles, to emphasize the unusual richness of the TC⁴ measurement suite and, in particular, the plume ages represented. Of note here, since the same airborne platform was involved, is the NASA DC-8 encounter with a stratospheric volcanic cloud ~33–35 h after the February 2000 eruption of Hekla (Iceland) during the SAGE III Ozone Loss and Validation Experiment (SOLVE I) [*Rose et al.*, 2003, 2006]. The encounter yielded a unique data set that was used by *Rose et al.* [2006] to model volcanogenic polar stratospheric cloud (PSC) formation and O_3 depletion in the volcanic cloud. More recently, *Oppenheimer et al.* [2010] have reported in situ measurements of the plume from Erebus volcano (Antarctica) in an instrumented Twin Otter aircraft, which also show evidence for in-plume O_3 destruction. We stress however, the distinction between the polar stratospheric and Antarctic environments of these encounters and the tropical tropospheric setting of the TC⁴ measurements. Given that the global distribution of volcanoes peaks in tropical latitudes [*Simkin and Siebert*, 1994], and that many of the strongest volcanic sources of SO_2 are located there [*Andres and Kasgnoc*, 1998], an understanding of the atmospheric chemistry of tropical volcanic plumes (and sulfur chemistry in particular) is of fundamental importance to volcanology and atmospheric science.

[7] With the exception of the studies cited above, direct volcanic plume sampling from aircraft has been rare since the 1990s. One of the earliest airborne volcanic plume sampling efforts targeted quiescent plumes from Kilauea (Hawaii), Arenal (Costa Rica) and Mayon (Philippines), finding mostly dilute sulfuric acid droplets 0.1–1 μm in size [*Cadle et al.*, 1969]. Beginning in the 1970s, the University of Washington Cloud and Aerosol Research Group (http://carg.atmos.washington.edu/) instigated many pioneering airborne volcanic plume sampling campaigns. Both quiescent volcanic plumes and particle-rich explosive eruption clouds were targeted, but chiefly at midlatitude or high-latitude volcanoes (e.g., Mt. Baker, Redoubt and Mt. St. Helens; USA) [*Radke et al.*, 1976; *Hobbs et al.*, 1982, 1991].

[8] Central American volcanoes were the targets of several in situ plume sampling campaigns in the 1970s–1980s [*Cadle et al.*, 1979; *Lazrus et al.*, 1979; *Rose et al.*, 1980; *Smith et al.*, 1982; *Phelan Kotra et al.*, 1983; *Casadevall et al.*, 1984]. *Rose et al.* [1980] summarize the characteristics of particles sampled in emissions from Pacaya, Fuego and Santiaguito volcanoes in Guatemala. Acid droplets, silicate glass fragments and crystal fragments comprised the small (<25 μm) particle fraction, with fragments often acid coated. Crystal-rich magmas were found to produce bimodal size distributions in the 0.04–25 μm diameter range, with modes at 0.2–0.8 μm and 3–10 μm consisting mostly of glass fragments and crystal fragments (crystals fractured on cleavage planes), respectively. *Rose et al.* [1980] concluded that crystal-rich magmas might produce more submicron-sized ash than aphyric magmas. SO_2 mixing ratios in the Guatemalan plumes ranged from 20 to 6400 ppb, and reported plume penetrations occurred no more than 35 km from the vent [*Lazrus et al.*, 1979], which we surmise to represent plume ages of no more than 5 h. A NASA Lockheed Electra aircraft intercepted quiescent plumes from Poás (Costa Rica), Arenal and Colima (Mexico) in February 1982 [*Casadevall et al.*, 1984]. The lower tropospheric plumes (<4 km altitude; 0.8–1.1 km thick) were sampled 1–20 km from the source volcanoes, which were discharging 2.3–8.1 kg s⁻¹ of SO_2. The maximum plume age sampled was ~2 h, based on the lowest reported wind speed. SO_2 mixing
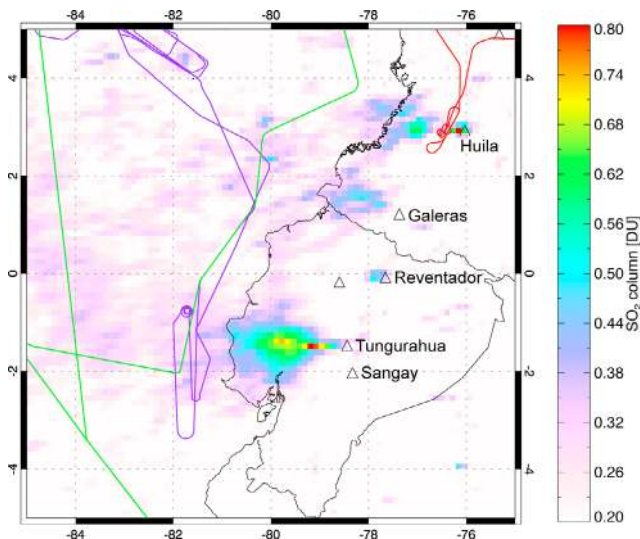
Figure 1. DC-8 flight tracks in the Ecuador/Colombia region during TC[4], superimposed on a map of average SO_2 column amounts measured by OMI over the period 16 July to 8 August 2007. Flights on 17 July (purple), 21 July (red), and 29 July (green) included volcanic plume penetrations. Volcanoes exhibiting SO_2 degassing in this period are Nevado del Huila (2.93°N, 76.03°W) and Galeras (1.22°N, 77.37°W) in Colombia and Reventador (0.08°S, 77.67°W) and Tungurahua (1.47°S, 78.44°W) in Ecuador.

ratios measured within the plumes were generally 10–260 ppb (with a maximum of 1900 ppb) at Colima. Particles were mostly <3 μm in aerodynamic diameter (with a mode at 0.1–0.3 μm) and consisted of droplets of dilute sulfur-bearing solutions and rare silicate particles coated with sulfur-bearing films or crusts, plus Ca, K and Na sulfate mineral fragments. *Casadevall et al.* [1984] suggested that small particle size and a unimodal PSD served to distinguish quiescent plumes from eruption plumes.

[9] *Mather et al.* [2003a] provide a review of tropospheric volcanic aerosol characteristics and sampling techniques. A number of recent studies have employed cascade impactors and filter packs to collect volcanic plume particles for size-resolved compositional analysis [e.g., *Mather et al.*, 2003b, 2004a; *Martin et al.*, 2008, 2009]. *Mather et al.* [2004a] report PSDs derived from sun photometry in quiescent plumes from Lascar and Villarrica (Chile). The maximum plume ages sampled were ~70 min at Villarrica and ~150 min at Lascar. Retrieved PSDs were bimodal with maxima at diameters of 0.2–0.4 μm and 1.4–3 μm, and concentrations of soluble SO_4^{2-} and NH_4^+ were well correlated with a mode at ~1 μm at Lascar's summit [*Mather et al.*, 2004a], indicating near-source aerosol neutralization.

[10] Near-source aerosol plumes produced by passive degassing at volcanoes with relatively accessible vents such as Etna (Sicily) and Masaya (Nicaragua) are also favorable sites for particle sampling. At Masaya, *Mather et al.* [2003b] determined near-source, size-resolved particle composition and found a PSD mode at a diameter of 0.5 μm correlated with soluble SO_4^{2-} and NH_4^+ concentrations. Neutralization of the acidic volcanic aerosol by ammonia was already evident at the crater rim and increased downwind [*Mather*

et al., 2003b]. Sampling of more aged tropospheric volcanic plumes is uncommon. A ~12 h old plume from Miyake-jima (Japan) was sampled ~170 km downwind in September 2000, from the summit of Mt. Fuji [*Naoe et al.*, 2003]. A high fraction of sulfuric acid containing particles (with no nonvolatile components) was observed in the 0.03–0.2 μm radius range when winds were from the direction of the volcano, indicating the influence of volcanic emissions on accumulation mode aerosol. Miyake-jima's emissions were also sampled 330 km north of the volcano in 2000–2001 [*Satsumabayashi et al.*, 2004], representing plume ages of ~12–18 h. Arrival of volcanically influenced air masses was indicated by increases in SO_2 and SO_4^{2-} concentrations in aerosol and precipitation, and decreased aerosol concentrations of nitrate (NO_3^-) and chloride (Cl^-) [*Satsumabayashi et al.*, 2004]. The SO_2 to sulfate conversion rate was 1% h^{-1} on average; twice as fast during the day as at night.

[11] *Mather et al.* [2003a] provide a summary of PSDs determined in volcanic plumes using various techniques. Multimodal PSDs are typical, reflecting contributions from

Table 1. Subset of the NASA DC-8 Payload During the TC⁴ Mission

Measurements	Experiment[a]	TC⁴ PIs
SO_2, H_2O_2, $HNO_{3(g)}$	CIMS	P. Wennberg, J. Crounse
SO_2, fine aerosol SO_4^{2-}, HNO_3	SAGA	J. Dibb
CO, CH_4	DACOM	G. Diskin, G. Sachse
CO_2	AVOCET	S. Vay
O_3	FastOz	M. Avery
NO, NO_2, HNO_3	TD-LIF	R. Cohen
Condensed water/ice content	CVI	C. Twohy, D. Rogers
Aerosol optical properties and size distribution: hot/cold condensation nuclei (CN) counters; Aerodynamic Particle Sizer (APS), $0.5 < D_p < 20$ μm; optical particle counter (OPC), $0.3 < D_p < 10$ μm; Ultra-High Sensitivity Aerosol Spectrometer (UHSAS), $0.06 < D_o < 1$ μm[b]	LARGE	B. Anderson
Single-particle composition (for $D_p > 0.2$ μm)[b]	PALMS	D. Murphy, K. Froyd
Aerosol and O_3 remote profile measurements	DIAL	J.W. Hair, E.V. Browell
Cloud particle size/type (~10 $< D_g < 2500$ μm)[b]	CPI	P. Lawson
Nadir and forward video	DC-8 Cam	R. Shetter
DC-8 navigation data	REVEAL	S. Gaines

[a]Techniques and pertinent references: CIMS, Chemical Ionization Mass Spectrometer [*Huey*, 2007]; SAGA, Soluble Acidic Gases and Aerosol (mist chamber/ion chromatograph) [*Scheuer et al.*, 2003]; DACOM, Differential Absorption CO Measurement [*Sachse et al.*, 1987]; AVOCET, Atmospheric Vertical Observations of CO_2 in the Earth's Troposphere [*Vay et al.*, 2003]; FastOz, in situ Fast-response Ozone measurements via Nitric Oxide Chemiluminescence [*Pearson and Stedman*, 1980]; TD-LIF, thermal dissociation–laser induced fluorescence [*Day et al.*, 2002]; CVI, Counter-flow Virtual Impactor [*Twohy et al.*, 1997]; LARGE, Langley Aerosol Research Group Experiment; PALMS, Particle Analysis by Laser Mass Spectrometry [*Murphy et al.*, 2006]; DIAL, differential absorption lidar [*Browell et al.*, 1983]; CPI, Cloud Particle Imager [*Lawson et al.*, 2001].

[b]D_p, aerodynamic diameter; D_o, optical diameter; D_g, geometric diameter. D_p represents the diameter of a sphere of unit density (1 g cm^{-3}) that has the same gravitational settling velocity as the particle in question.

gas-to-particle conversion in the accumulation mode (0.1–2 μm diameter) and from magma fragmentation and vent erosion in the coarse mode (>2 μm diameter). The relative dominance of these modes depends on the style of volcanic activity; explosive eruption plumes being richer in coarse particles than quiescent plumes. PSDs are expected to evolve during volcanic plume transport and as activity fluctuates, with preferential deposition of the coarse mode, although, as the summary above indicates, there have been few in situ measurements of tropospheric volcanic plumes more than a few hours in age.

[12] We provide here an overview of the TC[4] volcanic plume data set, highlighting some aspects of particular relevance to prior studies of volcanic plume chemistry. One aspect we wish to emphasize is the new insight into aged plumes provided by the observations. We begin by summarizing reported volcanic activity in the TC[4] footprint during the experiment; and then describe the DC-8 payload and measurements. In section 4 we examine the likely source volcanoes for the sampled plumes using a trajectory model. The volcanic plume penetrations west of Ecuador and over Colombia are described in detail in sections 5 and 6, respectively. Section 7 concerns the application of the TC[4] data to validation of OMI SO_2 measurements; and we conclude with a discussion that highlights some notable features of the data set with respect to sulfur, O_3 and NO_y chemistry.

2. Volcanic Activity in Ecuador and Colombia During TC[4]

2.1. Ecuador

[13] Several active volcanoes in Ecuador produce frequent gas and aerosol emissions (Figure 1). Tungurahua (1.47°S, 78.44°W, alt. 5023 m) has been continuously active since 1999, and exhibits cycles of activity evident in variable SO_2 emissions [e.g., *Carn et al.*, 2008; *Arellano et al.*, 2008]. In July 2007, continuous emission of ash-laden plumes near vent altitude was reported, with occasional larger explosive events producing ash columns up to 3 km above the vent [*Smithsonian Institution*, 2008a], and SO_2 emission rates of 1000–2000 tons per day (t d^{-1}; ~12–23 kg s^{-1}) were typical. Although Tungurahua was expected to be the main source of volcanic material sampled west of the Ecuadorian cordillera, both Reventador (0.077°S, 77.66°W, alt. 3562 m) and Sangay (2.00°S, 78.34°W, alt. 5230 m) are also persistently active. Elevated SO_2 columns were detected in a localized region near Reventador by OMI during TC[4] (Figure 1), although the eastern cordillera of Ecuador (where Reventador is located) is frequently cloud covered and significant cloud processing of emissions is likely (June–August is the wet season in the eastern cordillera). Plumes from Sangay were reported to altitudes of 5.2–8.2 km on 23, 24 and 28 July 2007, but no SO_2 or ash was detected in satellite imagery (Figure 1) [*Smithsonian Institution*, 2008b]. MODIS thermal anomalies were also recorded at Sangay by the MODVOLC system (http://modis.higp.hawaii.edu) on 18, 22 and 29 July, indicating ongoing activity.

[14] DC-8 flights off the Pacific coast of Ecuador were conducted on 17 and 29 July; corresponding flight paths are shown in Figure 1. Closer approaches to Tungurahua were precluded by air traffic control restrictions over Ecuador. The 17 July volcanic plume sampling occurred close to the time of the Aura satellite overpass to attempt validation of OMI SO_2 measurements. The DC-8 flew a descending spiral pattern to sample a vertical profile of the volcanic outflow (Figure 1).

2.2. Colombia

[15] The ice-capped Nevado del Huila volcano (2.93°N, 76.03°W, alt. 5364 m) produced its first eruption since the 16th century in February 2007. In July 2007, degassing occurred from fractures along Huila's glaciated summit ridge that opened up in February and April 2007. SO_2 emission rates ranging from 3000 to 14000 t d^{-1} (~35–162 kg s^{-1}) were measured sporadically from April through early June 2007 by INGEOMINAS (http://intranet.ingeominas.gov.co/popayan/Página_Principal), although no SO_2 emission rate measurements were made during TC[4]. Activity updates from INGEOMINAS are available for the time of the TC[4] mission, and report low seismic activity. Galeras volcano (1.22°N, 77.37°W, alt. 4276 m), located south of Huila, also degasses near continuously and SO_2 was measured west of Galeras by OMI during TC[4] (Figure 1). INGEOMINAS (http://intranet.ingeominas.gov.co/pasto/Página_Principal) reported SO_2 fluxes of 336–417 t d^{-1} on 19 July 2007, with the plume transported west of the volcano (no indication of plume altitude was given), and low seismicity during 17–22 July. The DC-8 penetrated Huila's emission plume ~35–50 km downwind of the volcano on 21 July (Figure 1).

3. NASA DC-8 Payload During TC[4]

[16] A summary of the NASA DC-8 payload during TC[4] is given in Table 1. The entire TC[4] data archive, including all measurements discussed herein, is accessible at: http://espoarchive.nasa.gov/archive/arcs/tc4/. A complete description of the instruments, measurements and associated uncertainties is not given here, but can be found in the references given in Table 1 and in the TC[4] data archive. Here we give an overview of the DC-8 measurements, focusing on those most useful for volcanic plume identification.

[17] An elevated SO_2 volume mixing ratio (vmr) measured by CIMS was used as the primary indication of volcanic plume penetrations, with elevated sulfate aerosol concentrations indicative of more aged plumes. CIMS SO_2 measurements have uncertainties equivalent to ±(50% of measured value plus 175 pptv). All CIMS data are 0.5 s averages sampled every ~10 s. The SAGA experiment (Table 1) measured mixing ratios of fine sulfate aerosol (<1 μm) integrated over sampling intervals of 83–91 s, with a detection limit of 5 pptv, and also provided bulk aerosol composition data (soluble ions) from filter samples.

[18] The NASA Langley Research Center (LARC) LARGE instrument suite (Table 1) provided measurements of aerosol optical properties and size distributions. CN includes particles that form droplets at supersaturations of over 400%, i.e., all available particles. CN data are subdivided into total CN, cold (or volatile) CN (>0.01 μm; mostly sulfates) and hot (refractory or nonvolatile) CN (>0.01 μm); the latter obtained with the sample heated to 300°C (includes soot, sea salt, mineral dust and volcanic ash). Ultrafine CN (0.003–0.01 μm; also termed nanoparticles) is equal to the difference between total CN and cold CN. Aerodynamic diameters (D_p) were converted to geometric diameters (D_g)

Table 2. NASA DC-8 Volcanic Plume Penetrations During the TC^4 Campaign in July 2007

Date	Time (UTC)	Location[a]	Pressure Altitude[a] (m)	Max. SO$_2$ (ppbv)	Plume[b]	Potential Source Volcano(es)	Plume Age[c] (h)
17 Jul	1730–1733	0.83°S, 81.69°W	4152	4.58	1	Tungurahua, Sangay, Reventador	~30–33, ~24–33
17 Jul	1734–1737	0.76°S, 81.65°W	3154	1.09	2	Tungurahua	~24–30
17 Jul	1823–1831	1.01°S, 81.46°W	3956	1.66	3	Tungurahua, Sangay	~24–30
17 Jul	1832–1837	0.27°S, 81.11°W	4351	2.05	4	Tungurahua, Sangay, Reventador	~43–48, ~22–31
21 Jul	1502–1506	3.03°N, 76.47°W	4912	94.62	5	Nevado del Huila	~2
29 Jul	1654–1704	1.80°S, 83.20°W	3427	0.72	6	Tungurahua, Sangay	~23–30
29 Jul	1712–1730	0.57°S, 81.55°W	5800	1.08	7	Tungurahua, Reventador	~29–36, ~25–35

[a]Corresponds to maximum SO$_2$ vmr measured by CIMS in the plumes.
[b]Provided for ease of reference in the text discussion.
[c]Where two age ranges are reported, the first assumes Tungurahua or Sangay as the source, and the second assumes Reventador as the source.

using $D_p = (\rho/F)^{1/2} \times D_g$, where ρ is density and F is the particle shape factor ($F = 1$ for spherical particles ($F = (b + c)/2a$, where a, b, and c represent the long, intermediate, and short particle axes, respectively)) [e.g., *Wilson and Huang*, 1979]. The UHSAS was calibrated using latex spheres with a refractive index close to that of ammonium sulfate, which probably accounts for a large fraction of the accumulation mode aerosol in this case.

[19] UHSAS and APS data were merged to create aerosol size distributions for a size range of 0.06–5 μm, using APS data in the overlap region between the two instruments and adjusting the APS D_p values to D_g using appropriate densities and shape factors and the relationship for D_g given above. The coarse-mode particles ($D_g > 1$–2 μm; which may have been volcanic ash; see section 5.3) were assumed to be

similar to mineral dust, which has a shape factor of about 1.6 and a density of ~2.5. This correction shifted the APS diameters to about 22% smaller sizes. Note that there is significant uncertainty on the particle density and shape factor. A density of 2.4–2.6 g cm^{-3} is reasonable for non-vesicular basalt clasts [*Fisher*, 1964; *Brazier et al.*, 1982], but distal volcanic ash density can vary depending on composition [e.g., *Riley et al.*, 2003, and references therein]. Reported shape factors for distal volcanic ashfall from explosive eruptions range from 0.5 to 0.8 [*Wilson and Huang*, 1979; *Riley et al.*, 2003]. We consider vesicular pumice very unlikely in the volcanic plumes sampled during TC^4, as there were no major explosive eruptions in Ecuador or Colombia during the campaign. Tungurahua erupts andesite magma that may contain ~30 vol % of
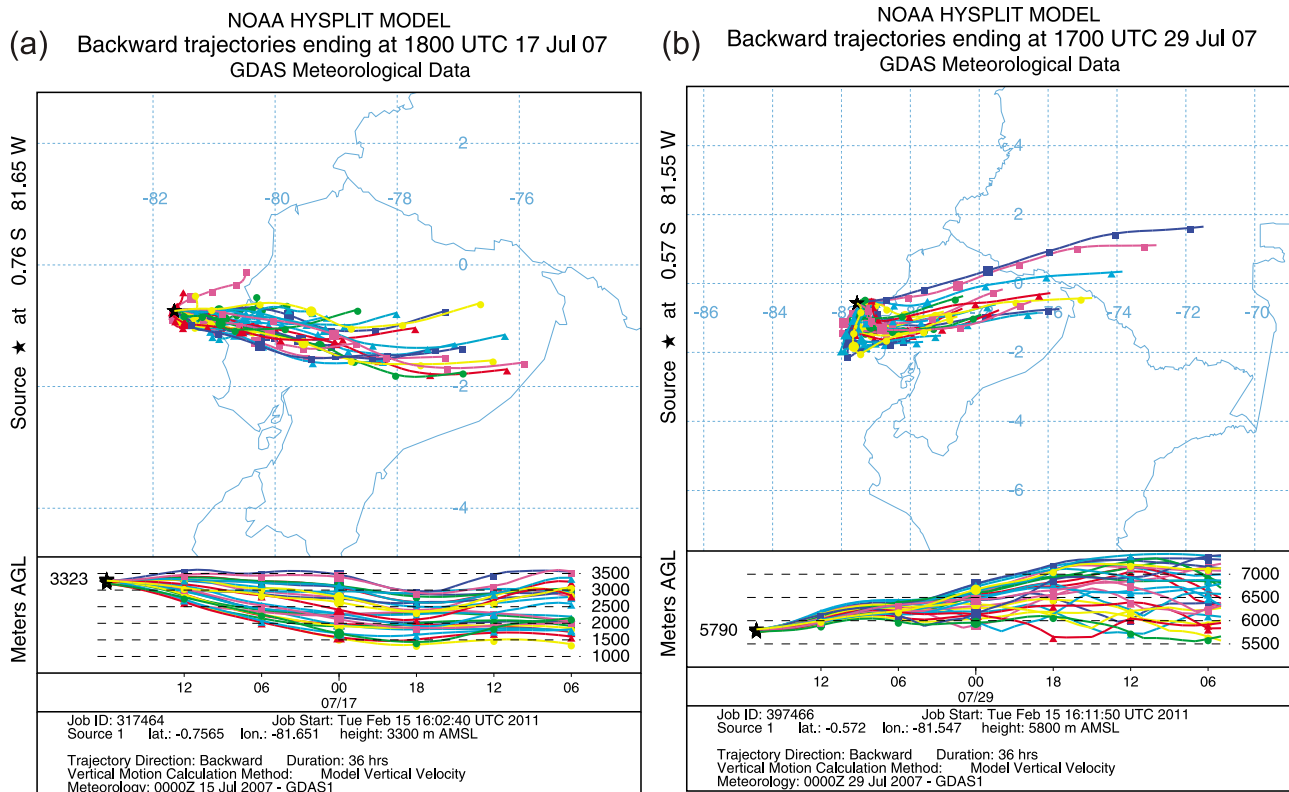
Figure 2. Examples of HYSPLIT ensemble back trajectories for volcanic plume penetrations, initialized at (a) 1800 UTC 17 July, 3300 m (plume 2) and (b) 1700 UTC 29 July, 5800 m (plume 7). Plume numbers correspond to those given in Table 2. See text (section 2) for the locations of degassing volcanoes.

plagioclase crystals [*Arellano et al.*, 2008], so crystal fragments might be supplied to the plumes by disruption of such magmas during weak explosive activity. Reventador's eruptive products are slightly less evolved and have included basaltic andesite [*Samaniego et al.*, 2008].

[20] The PALMS instrument (Table 1) measured single-particle composition as a function of particle size. Data products include mineral dust/ash fraction, which is the number fraction of aerosols detected by PALMS that are identified as mineral dust/ash. This is not a well-defined number concentration, but a relative measure of abundance. Relative sulfate mass fraction is a calibrated quantity corresponding to the relative amount of aerosol sulfate versus organic material, i.e., sulfate/(sulfate + organic). The PALMS $NH_4^+:SO_4^{2-}$ ratio is another calibrated quantity that is semi-quantitative and not well constrained above ∼2, but nevertheless this would indicate full neutralization of sulfate. The CPI probe (Table 1) complements PALMS through cloud particle sizing and imaging of particles.

[21] A zenith- and nadir-looking UV DIAL system was mounted in the DC-8 for remote vertical profiling of O_3, aerosols and clouds (Table 1). The DIAL measurements are averaged over a 450 m vertical range and 3 min time average (∼42 km). DIAL O_3 measurements were made using on- and off-line laser wavelengths of 291.5 and 299.6 nm, respectively, and their absolute accuracy is 10% or 2 ppbv, whichever is larger, and precision is 5% or 1 ppbv [*Browell et al.*, 2005]. DIAL aerosol measurements include the aerosol scattering ratio at 591 and 1064 nm (hereafter denoted ASR_{VS} and ASR_{IR}, respectively), defined as the ratio of attenuated aerosol backscatter to a modeled molecular backscatter. The volume (aerosol and molecular) depolarization ratio is the perpendicular divided by the parallel polarization components of the lidar signal referenced to the transmitted linear polarization, and the aerosol depolarization (ADP) is derived from the volume depolarization ratio and the ASR. ADP provides information on particle microphysics (e.g., shape), and it was calculated for $ASR_{VS} >$ 0.15. Aerosol wavelength dependence (AWD; see auxiliary material for plots of this parameter) for aerosol backscattering is sensitive to aerosol size and, to a lesser extent, shape and composition.[1] AWD values range from about zero to 4 with lower values representing larger aerosols (relative to the laser wavelength) and 4 representing particles of molecular dimensions. For all DIAL aerosol measurements the vertical resolution is 30 m, and horizontal averaging and reporting interval is 10 s (∼2.3 km at a DC-8 speed of 14 km/min). Aerosol discrimination using multiwavelength lidar is discussed further by *Sasano and Browell* [1989].

4. HYSPLIT Trajectory Modeling

[22] The presence of three active volcanoes in Ecuador (Tungurahua, Reventador and Sangay) meant that the source of the volcanic plumes sampled on 17 and 29 July was ambiguous, although we consider Tungurahua to be the dominant source. The Hybrid Single-Particle Lagrangian Integrated Trajectory (HYSPLIT_4) model (R. R. Draxler and G. D. Rolph, HYSPLIT (HYbrid Single-Particle Lagrangian

Integrated Trajectory) Model access via NOAA ARL READY Website, NOAA Air Resources Laboratory, Silver Spring, MD, 2003; available at http://www.arl.noaa.gov/ready/hysplit4.html, and G. D. Rolph, Real-time Environmental Applications and Display system (READY) Website, NOAA Air Resources Laboratory, Silver Spring, MD, 2003; available at http://www.arl.noaa.gov/ready/hysplit4.html) was used to calculate backward trajectories from locations of volcanic plume penetrations, to investigate possible contributions from Reventador and Sangay, and to assess the age of the sampled plumes (Table 2 and Figure 2). In Table 2 we distinguish seven individual plumes sampled during TC[4] based on spatial separation and/or significant differences in SO_2 and sulfate content. GDAS1/GFS meteorological data were used for the HYSPLIT runs. Back trajectories were initialized at the time (rounded to the nearest hour due to the time resolution of the model) and altitude of the maximum measured SO_2 vmr for each plume intercept on 17 and 29 July (Table 2). To evaluate the meteorological uncertainty associated with the trajectories, HYSPLIT was invoked in ensemble mode. In this mode, multiple trajectories are initialized from the selected starting location, and each member of the trajectory ensemble is calculated by offsetting the meteorological data by a fixed grid factor (one grid point in the horizontal and 0.01 sigma units in the vertical), resulting in 27 members for all possible offsets in X, Y, and Z.

[23] HYSPLIT trajectories (Figure 2) suggest that Tungurahua is the most likely source for the volcanic plumes sampled west of Ecuador, but in most cases contributions from Reventador and/or Sangay cannot be entirely ruled out (Table 2). Northward transport of air along the Ecuadorian coast is a feature of many trajectories (e.g., Figure 2). In the case of Reventador, back trajectory altitudes (>5.5 km, e.g., Figure 2b) are substantially higher than the vent altitude (∼3.6 km), suggesting that only significant explosive activity could have injected volcanic material into these air parcels. No such activity was reported in July 2007, but the eastern cordillera of Ecuador is persistently cloud covered throughout the June–August wet season and so activity reports are sparse.

5. Ecuadorian Volcanic Plume Penetrations

5.1. The 17 July Plume

[24] The DC-8 flew ∼50–125 km off the coast of Ecuador on 17 July, ∼300–400 km west of Tungurahua (Figure 1). DIAL profiles show prominent aerosol layers at ∼2–5 km altitude above a marine stratus cloud deck as the DC-8 overflew the volcanic outflow region (Figure 3). Layers detected at ∼2°N–3°N (e.g., at around 1600 UTC) are probably derived from Galeras and/or Huila volcanoes in Colombia. South of the equator, two distinct aerosol layers that we assume to originate from Tungurahua are apparent in the DIAL profiles at altitudes of ∼3 and 5 km; these layers merge southward, forming a fold-like structure open to the north (Figure 3). Both layers, shown in Figure 3, contained weakly depolarizing aerosol (ADP ∼10%–20%) with AWD values <1.5 (see auxiliary material), suggesting the presence of solid particles that are large relative to the DIAL wavelengths. AWD profiles show some evidence for stratification, with larger particles at lower altitudes (see auxiliary material).

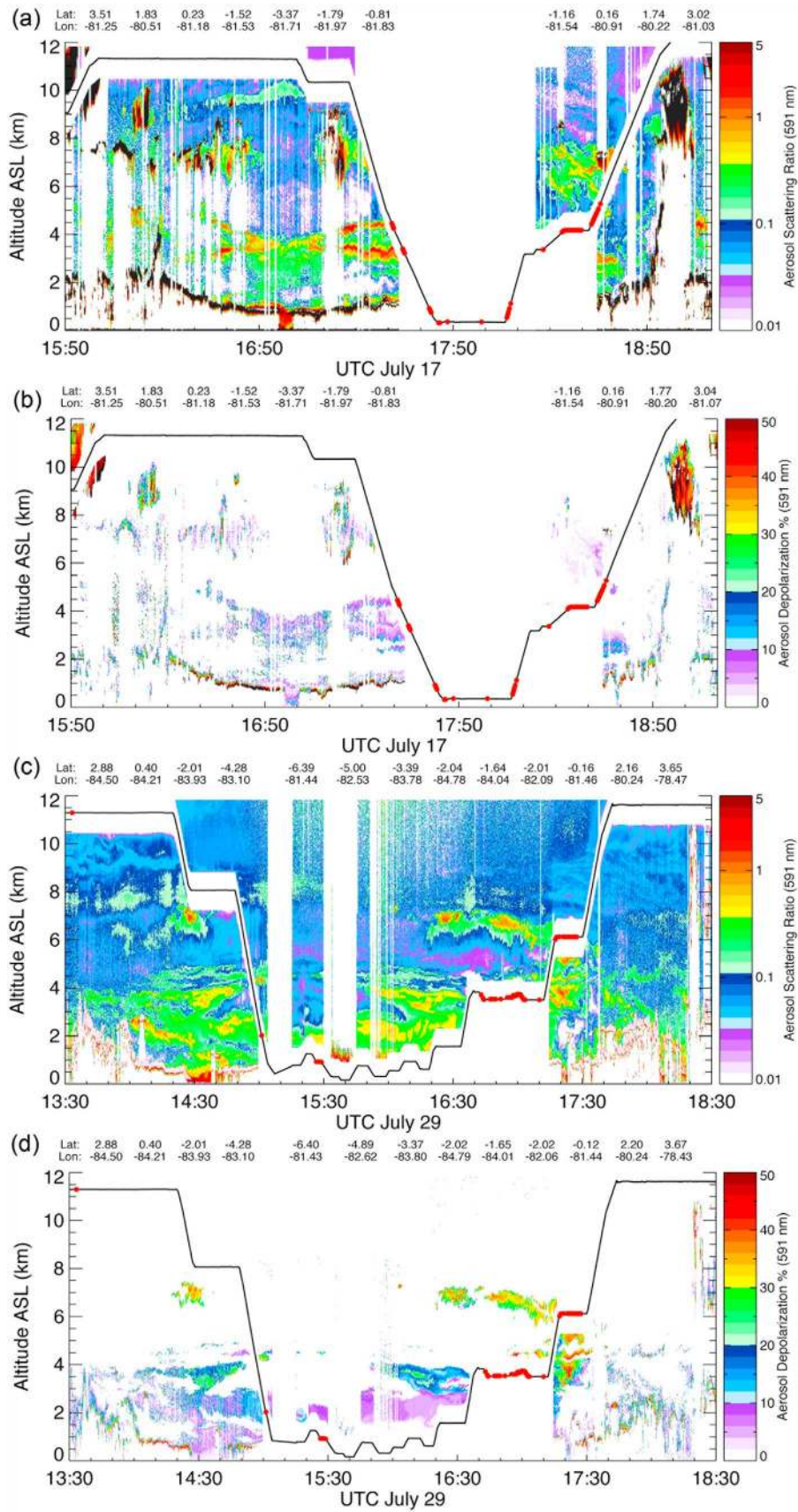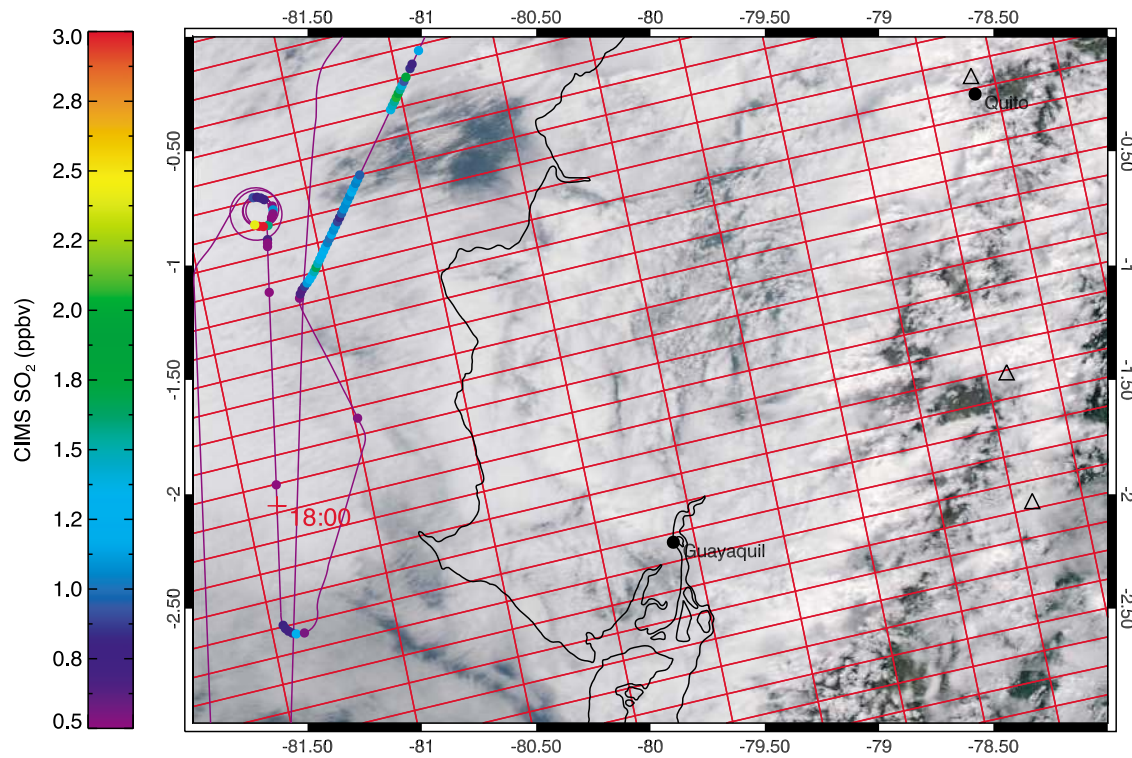**Figure 3**

Figure 4. SO₂ mixing ratios (≥0.5 ppbv) measured by CIMS (circular symbols) during the DC-8 flight off the Ecuadorian coast on 17 July at ~1730–1850 UT, superimposed on an Aqua/MODIS visible image collected at 1825–1830 UT. OMI ground-pixel boundaries for the 1843 UT Aura overpass are shown in red. Active volcanoes in Ecuador are indicated by triangles.

[25] The DC-8 executed a descending spiral pattern through the aerosol layers at ~0.75°S–0.85°S, 81.7°W, and measured elevated SO₂ vmrs in the core of both layers (Figures 3 and 4). The aircraft then sampled marine air in which SO₂ was also detected (we consider this unlikely to be volcanic SO₂ and it may represent ship emissions, SO₂ produced by oxidation of marine dimethyl sulfide (DMS), or pollution from the industrial city of Guayaquil), before ascending northward through the volcanic outflow (Figure 4). In situ data (Figure 5) collected during the descent show two layers with elevated SO₂ and sulfate (plumes 1 and 2; Table 2), with a higher $SO_2:SO_4^{2-}$ ratio in the upper, more SO₂-rich layer.

[26] The volcanic layers are also clearly delineated in CN data (Figure 5), most prominently by increased concentrations of cold CN, with minor increases in hot CN and localized peaks in ultrafine CN, i.e., a low hot CN/cold CN ratio. The highest CN counts (~7–9 × 10³ cm⁻³) occur in the higher-altitude plume (plume 1), which also contains the highest concentrations of ultrafine CN, presumably derived from ongoing SO₂ to aerosol conversion (binary nucleation

of sulfuric acid with water or ternary nucleation with water and ammonia). Particle counts seem to increase toward the base of each layer for plumes 1 and 2. The relative amounts of fine sulfate aerosol (measured by SAGA) and cold CN (which we assume to consist mostly of solid and aqueous ammonium sulfates) in these plumes may reflect the availability of NH₃ for neutralization of the volcanic sulfate. Data from the ascending pass through the volcanic plumes show similar features (Figure 5).

[27] A potentially significant feature of the 17 July data is a decrease in O₃ coincident with increased SO₂ and HNO₃, particularly in the upper layer (1731–1732 UT and 1832–1835 UT; Figure 5). This is discussed further in section 8.2. A particle-rich layer detected at 1845–1855 UT (Figure 5) appears to be not of volcanic origin, based on low SO₂ and sulfate content, and may represent Amazonian outflow influenced by biomass burning.

5.2. The 29 July Plume

[28] The Ecuadorian volcanic outflow was sampled again on 29 July, up to ~500–550 km WSW of Tungurahua and

Figure 3. DIAL profiles of (a) ASR$_{VS}$ (591 nm) and (b) aerosol depolarization (591 nm) on 17 July, 1550–1910 UTC (DC-8 flight 5), and (c) ASR$_{VS}$ (591 nm) and (d) ADP (591 nm) on 29 July, 1330–1830 UTC (DC-8 flight 10). The black line indicates the aircraft altitude, and red segments indicate where SO₂ ≥ 0.5 ppbv (Figures 3a and 3b) and SO₂ ≥ 0.3 ppbv (Figures 3c and 3d) was measured by CIMS. Geographic coordinates of selected waypoints are plotted above the profiles. Note scattering layers at altitudes of ~2–5 km (Figures 3a and 3b) and ~2–6 km (Figures 3c and 3d). There is a DIAL data gap from ~1730 to ~1820 UTC in Figures 3a and 3b due to the DC-8 being in a spiral descent and below the marine stratus clouds.
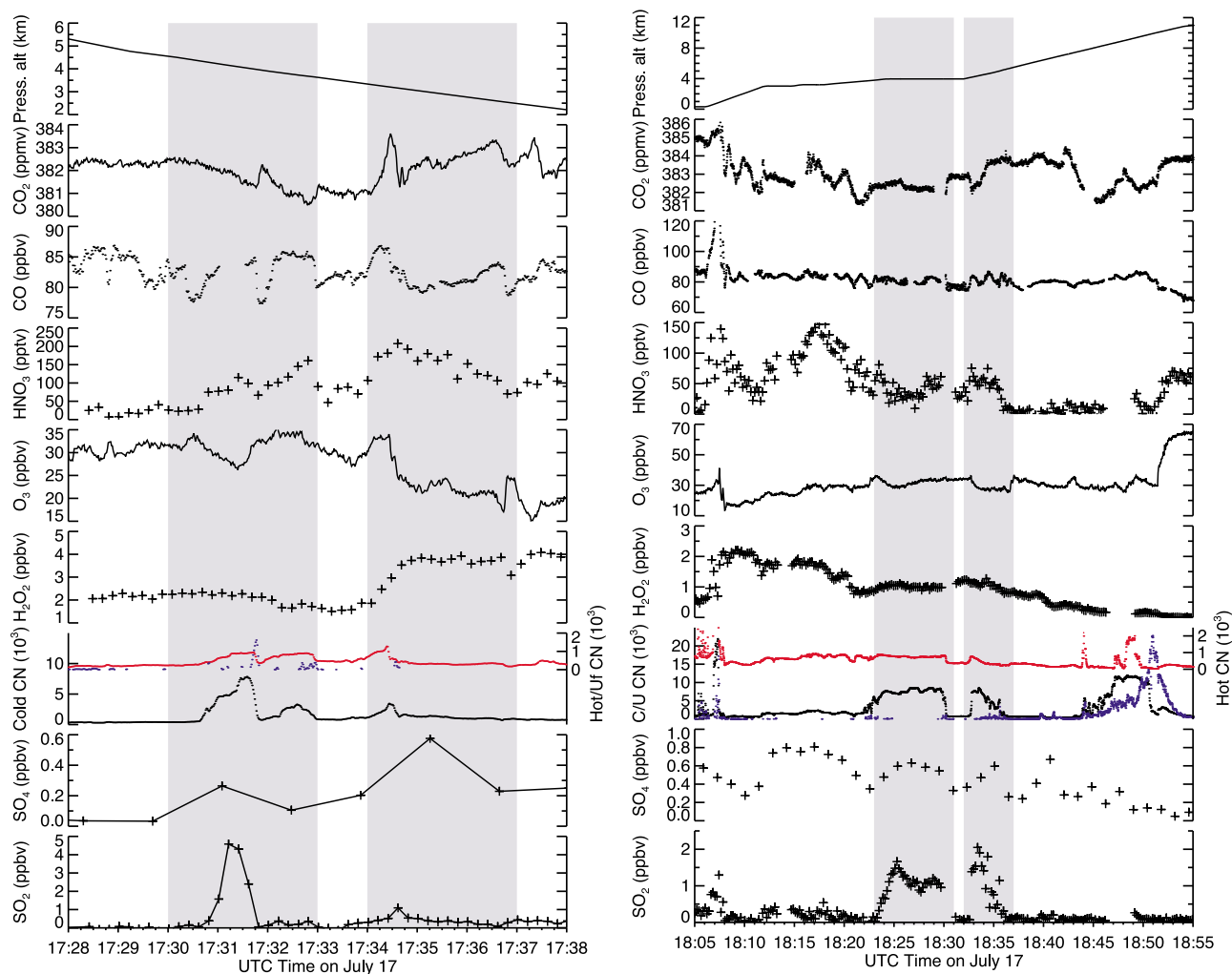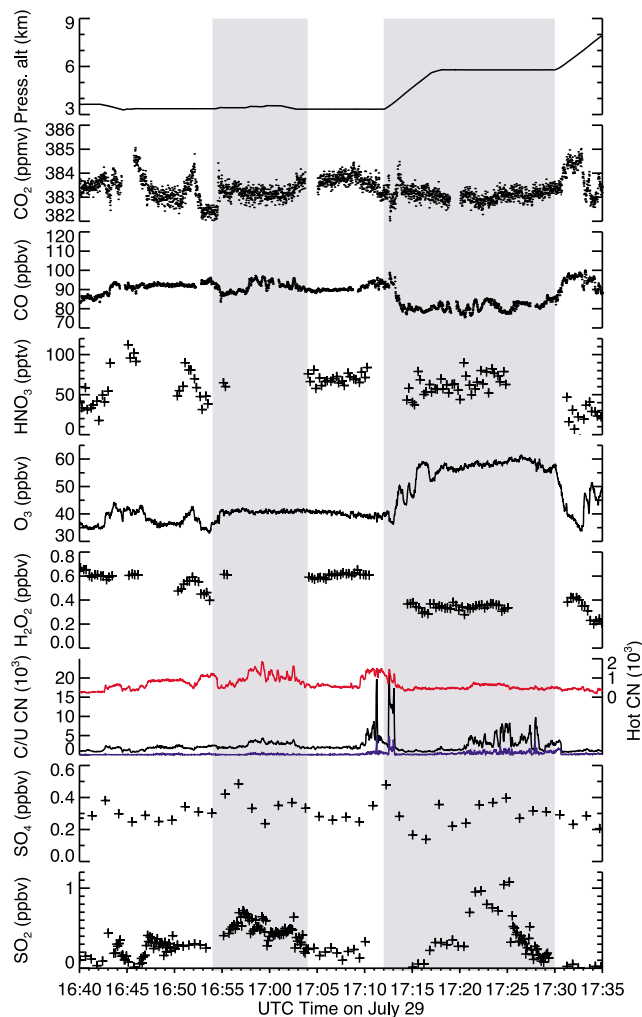
Figure 5. In situ measurements for volcanic plume penetrations on 17 July. From top to bottom, the parameters shown are DC-8 pressure altitude, CO_2 vmr, CO vmr, gas-phase HNO_3 vmr, O_3 vmr, H_2O_2 vmr, condensation nuclei (CN) number density (subdivided into cold (C; black), hot (red), and ultrafine (U; blue)), aerosol SO_4^{2-} vmr, and SO_2 vmr. Note that these are discrete measurements with variable sampling intervals and integration times; in some cases data points have been connected for clarity, but this does not imply continuous data. Shaded regions indicate plumes 1, 2, 3, and 4 referred to in Table 2.

also along a repeat of the 17 July flight path (Figure 1). DIAL profiles collected at ~84°W on the southward leg of the flight show volcanic aerosol layers at ~2–5 km altitude (Figure 3), similar to 17 July. However, since the plumes were profiled further downwind on 29 July, the ASR values are lower (particularly ASR_{VS}), ADP is higher, and AWD values indicate a shift toward larger particle sizes (perhaps due to accumulation of gas phase species; see auxiliary material). Very little SO_2 was detected during descent through the fringes of these layers at ~4.3°S (Figure 3). Also of note is a moderately depolarizing (ADP of 20%–40%) aerosol plume at 6–7 km altitude, which was sampled in situ later in the flight. The DC-8 turned toward Ecuador shortly after 1630 UTC and flew on a heading toward Tungurahua. Visible aerosol layers were noted in flight reports at this time (see auxiliary material).

[29] Slightly elevated SO_2 vmrs were measured on the approach toward the Ecuadorian coast at altitudes of 3–4 km

(Figure 6; plume 6 in Table 2). The aircraft turned north at ~82°W and ascended through the layer at ~6 km altitude, where slightly higher SO_2 vmrs were measured (Figures 3 and 6; plume 7 in Table 2). As for 17 July, $SO_2:SO_4^{2-}$ ratios are higher in the more SO_2-rich regions and the volcanic plumes are also distinctive in the CN data. In the layer sampled at 3–4 km altitude, cold CN counts are lower and hot CN counts higher relative to the plumes sampled on 17 July (Figure 6), although the altitude range sampled may have been a factor if the plumes were inhomogeneous and/or stratified. Plume heterogeneity is implied by the occurrence of two spikes in the CN data and increased SO_4^{2-} as the DC-8 turned and increased altitude at ~1710 UTC (Figure 6), when there was a short gap in CIMS SO_2 measurements. Elevated hot CN counts in plume 6 suggest the possible presence of refractory particles such as volcanic ash, which is also supported by PALMS data (see section 5.3); hot CN counts were lower in plume 7 at ~6 km altitude,

Figure 6. In situ measurements for volcanic plume penetrations on 29 July. From top to bottom, the parameters shown are DC-8 pressure altitude, CO_2 vmr, CO vmr, gas-phase HNO_3 vmr, O_3 vmr, H_2O_2 vmr, condensation nuclei (CN) number density (subdivided into cold (C; black), hot (red), and ultrafine (U; blue)), aerosol SO_4^{2-} vmr, and SO_2 vmr. Note CIMS (SO_2, H_2O_2, HNO_3) data gap from 1710–1715 UTC. Shaded regions indicate plumes 6 and 7 referred to in Table 2.

perhaps due to sedimentation of ash to lower altitudes. Ultrafine particle concentrations were low in the 29 July plumes (Figure 6).

[30] Plume 7 was embedded in an air mass with relatively high O_3 and low CO concentrations (Figure 6), which may indicate O_3 production by oxidation of CO (catalyzed by NO_x) in Amazonian outflow. The main CO source in this region in July is early dry season biomass burning in the Amazon rain forest, which raises the question of whether the SO_2 in this layer (~1 ppbv; Figure 6) could also be of biogenic origin. However, *Andreae and Andreae* [1988] report somewhat lower SO_2 mixing ratios in fresh biomass burning emissions over central Amazonia in July–August 1985 (averages of 27 and 18 ppt in the PBL and the free troposphere, respectively). Concentrations of aerosol sulfate and methanesulfonate were also relatively low (PBL

averages: 129 and 6 ppt, respectively) [*Andreae and Andreae*, 1988]; suggesting that the flux of biogenic sulfur from the Amazon Basin is insufficient to explain the SO_2 and SO_4^{2-} levels encountered during TC^4. Moreover, the presence of volcanic material at altitudes of 6 km and above is consistent with reports of intermittent explosive activity at Tungurahua (and Sangay) during late July 2007 (particularly after 18 July), injecting volcanic gases and ash to altitudes of ~8 km [*Smithsonian Institution*, 2008a, 2008b].

5.3. Aerosol Size Distributions and Composition
5.3.1. Aerosol Size Distributions

[31] Particle number, surface area and volume spectra for the Ecuadorian volcanic plume penetrations, derived from the LARGE instrument suite (Table 1), are shown in Figure 7.

[32] Aerosol size distributions have been analyzed by combining UHSAS data for particle diameters of 0.06–0.4 μm with APS data for particle diameters of 0.4–20 μm. Number distributions are dominated by ultrafine particles (usually defined as particles smaller than 0.1 μm in diameter) on 17 and 29 July, with similar particle counts on both days. All spectra show a mode at 0.1–0.2 μm (accumulation mode, condensation submode), which can be ascribed to SO_2-to-particle conversion in the plumes since the magnitude of this mode is inversely proportional to the peak SO_2 vmr measured in each plume (Table 2; see discussion in section 8.1). The 17 July spectra show a prominent mode at 0.5–0.6 μm that is only weakly evident in the 29 July data (Figure 7), and which is accentuated in the more sulfate-rich regions of the plumes. Based on PALMS data (see section 5.3.2; Figure 8a), this accumulation mode aerosol is an external mixture of coated ash and sulfate-organic particles, which is also consistent with the shapes of larger particles (>15 μm) imaged by the CPI probe (Figure 9). They are slightly larger than accumulation mode sulfate particles reported from other volcanic regions (e.g., downwind of Hawaii) [*Porter and Clarke*, 1997], but this could reflect a combination of factors including the age of the plumes sampled during TC^4, the ash component in the Ecuadorian plumes (ash being less common in Hawaiian volcanic emissions), particle hygroscopicity, or the coefficients used here to convert D_P values to geometric diameters.

[33] A distinctive feature of the 29 July spectra is a coarse mode aerosol component at diameters of ~2 μm (Figure 7). This is clearest in the plume sampled at higher altitude (plume 7). Based on PALMS data (see section 5.3.2), CPI images of angular aggregates >10 μm in diameter (more consistent with volcanic ash than cloud particles; Figure 9) and DC-8 camera images of brownish haze layers (see auxiliary material), we conclude that this represents a volcanic ash component in the plumes. This is also consistent with DIAL measurements of ADP (Figure 6) and AWD (see auxiliary material). LARGE data also show elevated hot CN (i.e., refractory aerosol such as ash or dust) in plume 6 on 29 July (Figure 6), when PALMS data show a much smaller volcanic ash or dust component (Table 3). Since PALMS only measures single-particle composition for D_p > 0.2 μm, one possible inference is that the lower-altitude layers furthest from Ecuador contained very fine ash (D_P < 0.2 μm). The presence of volcanic ash in Tungurahua's emissions would also be consistent with intermittent ash-bearing
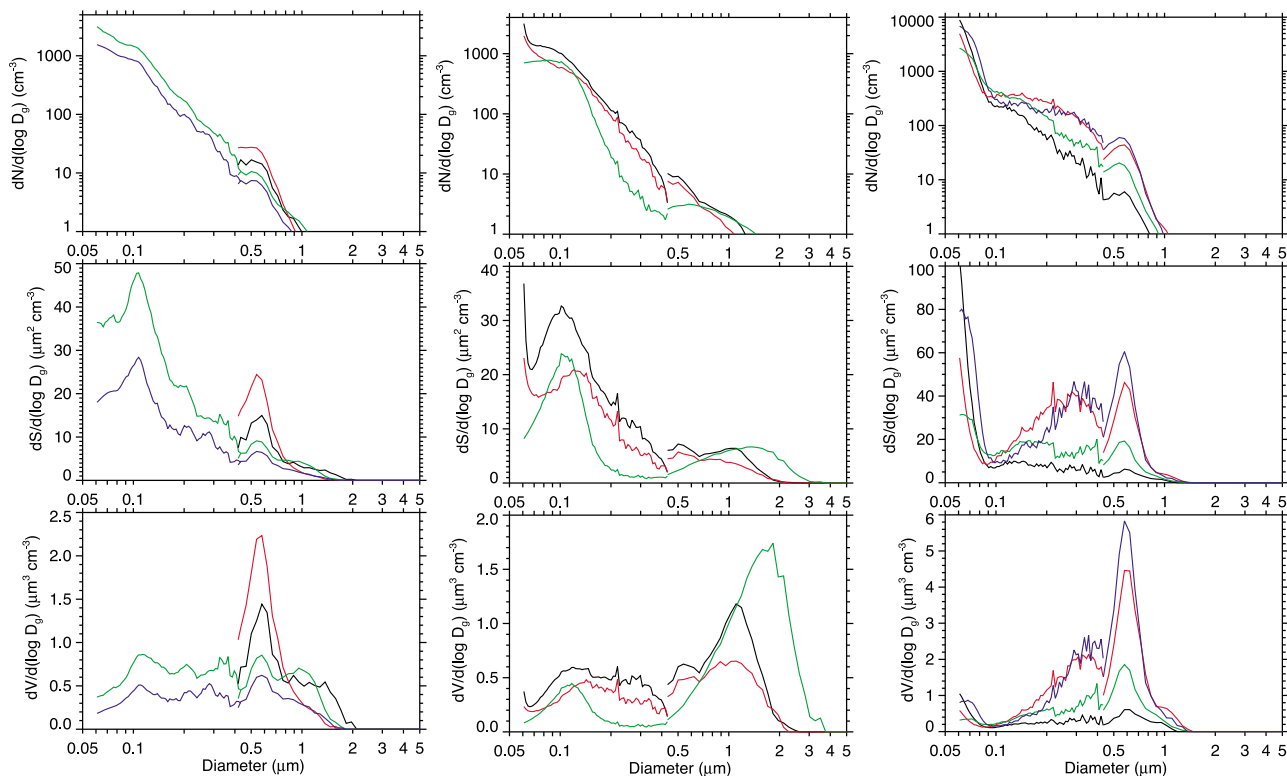
Figure 7. Average aerosol number, surface area, and volume distributions measured by UHSAS (0.06 μm < D_g < 0.42 μm) and APS (0.42 μm < D_g < 20 μm) for volcanic plume penetrations on 17, 21, and 29 July. APS aerodynamic diameters have been converted to geometric diameters (see section 3) assuming spherical particles. (left) Spectra for Ecuadorian plumes sampled on 17 July at (all times are UTC) 1730–1732 (black, APS only), 1732–1736 (red, APS only), 1823–1831 (green), and 1832–1837 (blue). The UHSAS data have been scaled by the ratio of the total counts to 90% of the CN number density owing to unreliable UHSAS counts. (middle) Spectra for Ecuadorian plumes sampled on 29 July at 1654–1707 (black), 1708–1715 (red), and 1715–1732 (green). (right) Spectra for Nevado del Huila plumes sampled on 21 July at 1501:30–1503 (black), 1504:10–1506 (red), 1507:45–1510:30 (green), and 1512:30–1514:15 (blue). The coarse mode volume is much lower than measured in the Ecuadorian volcanic outflow.

explosions and widespread ashfall reported at the volcano in late July 2007 [*Smithsonian Institution*, 2008a].
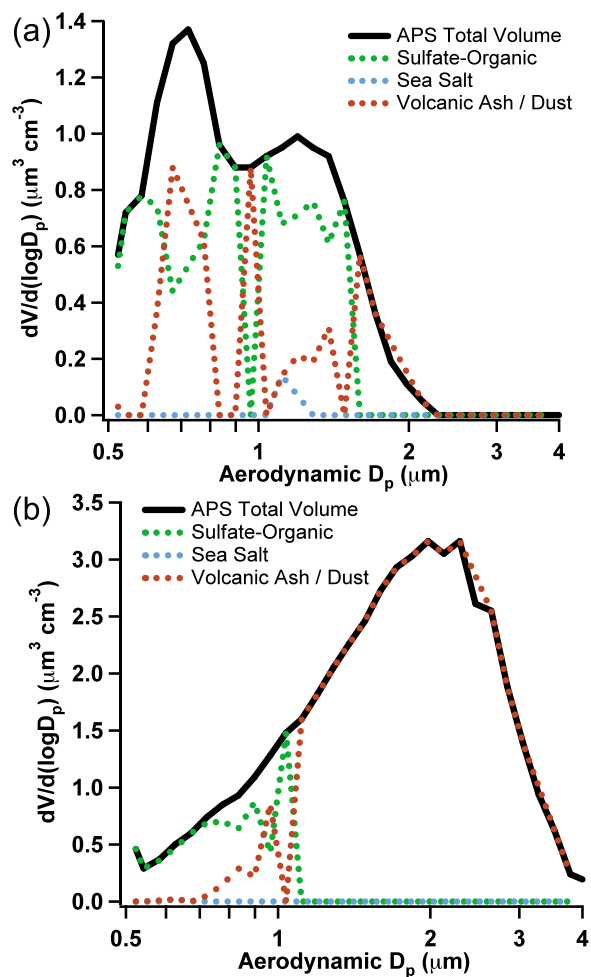
5.3.2. Aerosol Composition (PALMS)

[34] Volcanic plume particles were notably different than free tropospheric particles near the plumes (Table 3). We stress that plume penetrations were generally brief, which can result in poor statistics, particularly for large particle sizes where counts can be very low. All the volcanic plumes contained sulfate-rich accumulation mode particles that were often highly acidic. In the 29 July plume 7, the peak in sulfate content and sulfate acidity was not coincident with the maximum SO₂ vmr (Figure 10). These accumulation mode aerosols were essentially composed of pure sulfuric acid (with few organics or neutralizing components), which is rarely observed in the free troposphere (a $NH_4^+:SO_4^{2-}$ ratio of 2 or more indicates complete sulfate neutralization; Table 3 and Figure 10). This may reflect exhaustion of neutralizing ammonia in the highly acidic plume environment, as was observed downwind of Miyakejima volcano by *Satsumabayashi et al.* [2004].

[35] Elevated concentrations of large particles classified by PALMS as ash or mineral dust were sometimes observed,

in particular in plume 7 on 29 July (P_{alt} = 5.8 km; Table 3). Given that it would be very unusual to observe mineral dust in such concentrations at this latitude and altitude, coupled with the CPI observations of aggregate particles noted above, we interpret this as volcanic ash. It should be noted, however, that some of the larger aggregates in the CPI images (e.g., see 1700–1705 UT in Figure 9b) are in the region of the plume where micron-sized volcanic ash was not strongly enhanced (Table 3 and Figure 10). Elevated ash levels were observed spatially within and below zones of elevated SO₂ vmr. PALMS size-resolved particle composition data indicates that the coarse particle mode in the 29 July plume 7 was entirely volcanic ash (Figure 8b). Particles with D_p < 0.9 μm were predominantly sulfate-organic mixtures.

[36] The 29 July volcanic ash composition is broadly similar to mineral dust/ash of the background troposphere (based on a comparison with PALMS spectra collected during known mineral dust events), but with higher silicate levels and much lower organic content. Silicate-rich ash can result from depletion of metal ions in the acidic plume environment [e.g., *Delmelle et al.*, 2007], or a predominance of crystal fragments in the ash. Persistence of the >10 μm

Figure 8. APS average aerosol volume distribution (0.5 < D_p < 5 μm) and PALMS size-resolved, single-particle composition (D_p > 0.2 μm) for volcanic plume penetrations on 17 and 29 July. Individual particles are classified into three broad types: (1) biomass burning plus sulfate-organic internal mixtures; (2) mineral dust and volcanic ash (indistinguishable); and (3) sea salt. For each size bin, the fractional abundance of each particle type is multiplied by the APS volume in that bin, yielding a quantitative volume distribution for the three particle types (colored lines). (a) The 17 July, 1824–1836 UT plume penetration (plumes 3 and 4). PALMS composition indicates externally mixed ash and sulfate-organic particles up to 1.5 μm, above which ash dominates (not obvious here because of APS falloff at 2 μm). (b) The 29 July, 1712–1730 UT plume penetration. This corresponds to plume 7, the higher of two distinct plumes encountered on 29 July.

diameter ash particles detected by the CPI in the plume implies elevated porosity and low density to prevent ash fallout. Comparison of scatter heights and D_p values for the 1–4 μm ash particles suggests that they have density/shape factor ratios equal to or slightly higher than Saharan dust ($\rho = 2.6$; $F = 1.4$); that is, the ash is neither highly porous nor particularly dense. A few ash particles in the Ecuadorian volcanic plumes were found to contain Thallium, which is a rare observation but consistent with reports

of heavy metal enrichment (including Tl) in volcanic emissions elsewhere (e.g., Etna) [*Gauthier and Le Cloarec*, 1998].

[37] Small amounts of volcanic ash were also apparent in the 17 July plume (Table 3 and Figure 8a). Silicate levels were similar in the 17 and 29 July plumes, but ash from the 29 July plume 7 had higher iron levels than the 17 July plumes 3 and 4, suggesting a different source volcano (a possibility also implied by HYSPLIT back trajectories; section 4), and/or differences in the relative abundance of crystal fragments and volcanic glass. In addition to supermicron ash, a distinctive feature of the 17 July plume was a population of submicron aerosol that appeared to be ash or dust coated with sulfate (Figure 8a). Due to low particle counts on both days, this ash composition comparison is unavoidably tentative.

6. Huila Volcanic Plume Penetration

[38] The Huila volcanic plume was targeted during a DC-8 flight over Colombia on 21 July (Figure 1). An enhanced aerosol-laden plume with relatively low AWD (particles >1 μm in size) and weak ADP values was identified west of the volcano at altitudes of 4–5 km in the DIAL aerosol data (Figure 11; also see auxiliary material). It is unclear if the aerosols in this region, which were detected over the Cauca Valley west of Huila (Figures 11 and 12), originated from the volcano or from other sources, such as anthropogenic pollution related to the large industrial city of Cali (3.5°N, 76.4°W), or a combination of both. The DIAL O_3 measurements in the plume showed an apparent enhancement of about 30 ppbv over background values (Figure 11); however, the DIAL laser wavelengths at 291.5 and 299.6 nm are also sensitive to absorption by high levels of SO_2, and a concentration of about 90–100 ppbv SO_2 in the plume would yield about the same absorption as an additional 30 ppbv O_3. A maximum of ~100 ppbv SO_2 was measured in the plume by CIMS (Figure 13), but no enhanced O_3 was observed across the plume. This is consistent with the enhanced absorption observed remotely by DIAL and initially attributed to enhanced O_3 when it was actually due entirely to elevated SO_2 in the plume. Following the reconnaissance overflight, the DC-8 descended and penetrated the volcanic plume ~34–50 km downwind of the volcano, where the estimated plume age was ~2 h or less (Figures 11 and 12).

[39] The aircraft made two passes through the SO_2 plume (Figures 12 and 13); the first (~50 km from Huila) lasted ~56 s, which gives a sampling distance of ~8.4 km at the DC-8 air speed. The second penetration (34 km from Huila) lasted ~70 s, yielding a sampling distance of ~11.6 km. These two plume penetrations (combined as "plume 5" in Table 2) were separated by period of much reduced SO_2 (Figure 13) when the DC-8 entered a meteorological cloud, which is apparent in the MODIS image shown in Figure 12, and also clearly manifested by increased CWC in Figure 13. Significant convective cloud development over the Colombian cordillera is already apparent in the 1505 UTC MODIS image (Figure 12), and the region was almost completely cloud covered by the time of the afternoon Aqua MODIS and Aura OMI overpass at 1805–1820 UTC.

[40] In situ data show a slight increase in CO_2 vmr (<1 ppm) within the Huila plume, close to the SO_2 peak (Figure 13). The maximum CO_2 vmr in the plume is 382.9 ppm or ~0.6 ppm
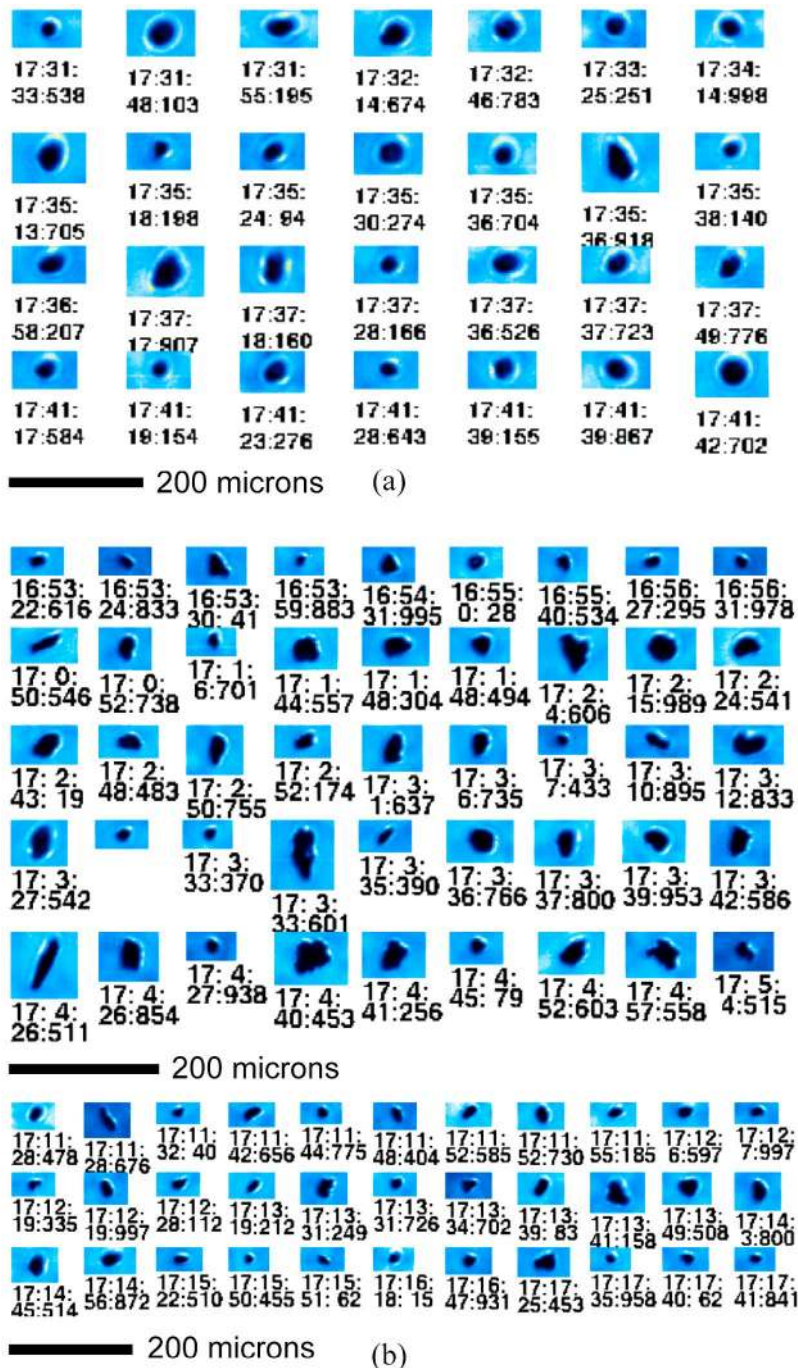
Figure 9. Representative CPI images of particles sampled during volcanic plume penetrations. Sampling time (UTC) is plotted below each image. (a) Particles sampled on 17 July at ~1731–1741 UT (plumes 1 and 2). Some subangular particles are evident, but most are spherical, indicating liquid or ash particles coated with sulfuric acid. (b) Particles sampled on 29 July at ~1653–1705 and ~1711–1719 UT (plumes 6 and 7). The images show notably angular particles or aggregates >10 μm in size. The highest PALMS ash fractions were measured from 1712 to 1730 (see Figure 10).

above local background. This could represent a small volcanic contribution to the local CO_2 burden. We have no other constraints on CO_2 emissions from Huila, but these mixing ratios are not unreasonable based on measurements at other volcanoes [e.g., *Gerlach et al.*, 1997, 1998; *McGee et al.*, 2001]. *Gerlach et al.* [1998] measured 0.3–0.6 ppm CO_2 in the Pu'u'O'o plume at Kilauea volcano (Hawaii). *Allard et al.* [1991] measured a mean CO_2 excess of 5 ppm at Etna (Italy) in 1984 (15 km from the crater), with a peak of ~10–20 ppm, but the Etna plume contained ~0.5 ppm SO_2, roughly 5 times more than the peak SO_2 vmr measured at Huila.

Table 3. Composition of Volcanic Plume Particles Measured by PALMS During TC[4]

Plume, Time, and Total Particles	Sulfate-Organic Plus Biomass Burning[a]	Volcanic Ash Plus Mineral Dust[a]	Sea Salt[a]	Sulfate Mass Fraction[b]	Organic Mass Fraction[b]	$NH_4^+:SO_4^{2-}$ Ratio[c]
		Tungurahua: 17 Jul 2007				
Plumes 3–4, 1824–1836 UT, n = 962	0.90	0.03	<0.01	0.80	0.20	0.6 (1.3)
		Tungurahua: 29 Jul 2007				
Plume 6, 1654–1704 UT, n = 804	0.95	0.02	<0.01	0.81	0.19	0.6 (1.9)
Plume 7, 1712–1730 UT, n = 471	0.84	0.14	<0.01	0.66	0.34	0.3 (0.45)
Near-plume region, n = 2362	0.93	0.02	<0.01	0.25	0.75	2.0
		Huila: 21 Jul 2007				
Plume 5, 1501–1511 UT, n = 119	0.96	0.02	<0.01	0.62	0.38	0.2 (1.1)

[a]Number fraction of particles within each particle type.
[b]Average sulfate and organic mass fractions of sulfate-organic plus biomass burning particles based on mass spectral calibrations [*Murphy et al.*, 2006].
[c]Average sulfate acidity expressed as equivalent $NH_4^+:SO_4^{2-}$ ratio [*Froyd et al.*, 2009]. Numbers in parentheses are obtained from bulk filter samples in and around the plumes (SAGA data).

6.1. Aerosol Size Distributions and Composition

6.1.1. Aerosol Size Distributions

[41] The volcanic plume penetrations are also clearly demarcated in CN data (Figure 13). The first passage through the plume (furthest from Huila, and at higher altitude) shows higher hot CN counts, and similar cold and ultrafine CN counts, to the second penetration (after flying through meteorological cloud). This could indicate some stratification of refractory particles in the volcanic plume (perhaps due to absorption and self-lofting), but plume heterogeneity caused by variable source emissions is equally plausible. Particle size spectra (Figure 7) show particle number densities (total CN counts up to ~20 × 10^3 cm^{-3}) significantly higher than encountered in the Ecuadorian volcanic outflow, in accordance with the relative ages of the plumes. The Huila spectra show accumulation mode aerosol peaking at a diameter of ~0.6 μm, but the 0.1 μm mode present in the Ecuador data is absent (Figure 7), and Huila's plume appears to lack significant coarse aerosol (D_g > 1–2 μm). The younger section of the Huila plume (red and green curves in Figure 7) contains more particles >0.1 μm in diameter, and overall higher aerosol volume than the more aged plume (see below). Reasons for this could include progressive loss of particles downwind due to fallout, cloud processing of the plume, or aerosol stratification. In view of the pervasive cloud cover at the time (note that the summit of Huila is cloud covered in Figure 12, implying that emissions were entrained directly into clouds) we suspect that cloud processing (e.g., through a nonprecipitating cloud cycle) probably influenced particle evolution in the Huila plume, depending on which particles were activated as CCN.

[42] Note that two more volcanic plume penetrations are evident in the CN data at 1508–1511 UTC and 1512–1514 UTC, although no CIMS SO_2 data were collected in this interval (Figure 13). These are additional transits through the Huila plume as the DC-8 circled and flew northward (note the flight path in Figure 12). It is noteworthy that sulfate aerosol concentrations are highest in the final plume penetration, which occurred in a similar location to the meteorological cloud encountered at 1503–1504 UTC. Aerosol size spectra indicate that this plume segment also contained the highest aerosol volume (Figure 7). This may represent an observation of the immediate effect of cloud processing and aqueous phase oxidation of SO_2 (see sections 6.2 and 8.1) to produce sulfate aerosol, which is known to have significant effects on aerosol size distributions [e.g., *Hoppel et al.*, 1994].

6.1.2. Aerosol Composition

[43] PALMS detected no significant ash or mineral dust component in the Huila plume (Table 3), despite the proximity to the volcano, likely due to the style of volcanic activity and a lack of significant ash emissions. The Huila particles had the lowest sulfate mass fraction and highest organic content of all the sampled volcanic material (Table 3), consistent with the young age of this plume. They show some neutralization by ammonia, but were the most acidic of all plume particles sampled (Table 3). Signatures of elemental sulfur were also evident in particle spectra, which was unique to the Huila plume. The detection of hot CN in the Huila emissions by LARGE and low abundance of volcanic ash in PALMS data could mean that very fine ash (<0.2 μm) was present. No explosive activity was reported at Huila during TC[4], but a small quantity of fine ash or other refractory material in the emissions would not be surprising. *Martin et al.* [2009] discuss the possible origin of fine silicate particles in quiescent volcanic plumes, which can include magma spattering and bubble bursting at the surface of a low-viscosity magma column (unlikely in the Huila case), condensation from Si-rich vapors, or the entrainment of wall rock fragments and/or fumarole encrustations into the gas flow. PALMS would still classify such exotic particles as ash/dust if they contained common metals or semimetals.

6.2. Cloud Processing of SO_2

[44] Transit through a meteorological cloud is clearly shown by increased CWC in Figure 13, which is presumed to be mostly liquid water at 4–5 km altitude in the tropics. At the same time, SO_2 and H_2O_2 levels drop to near zero,
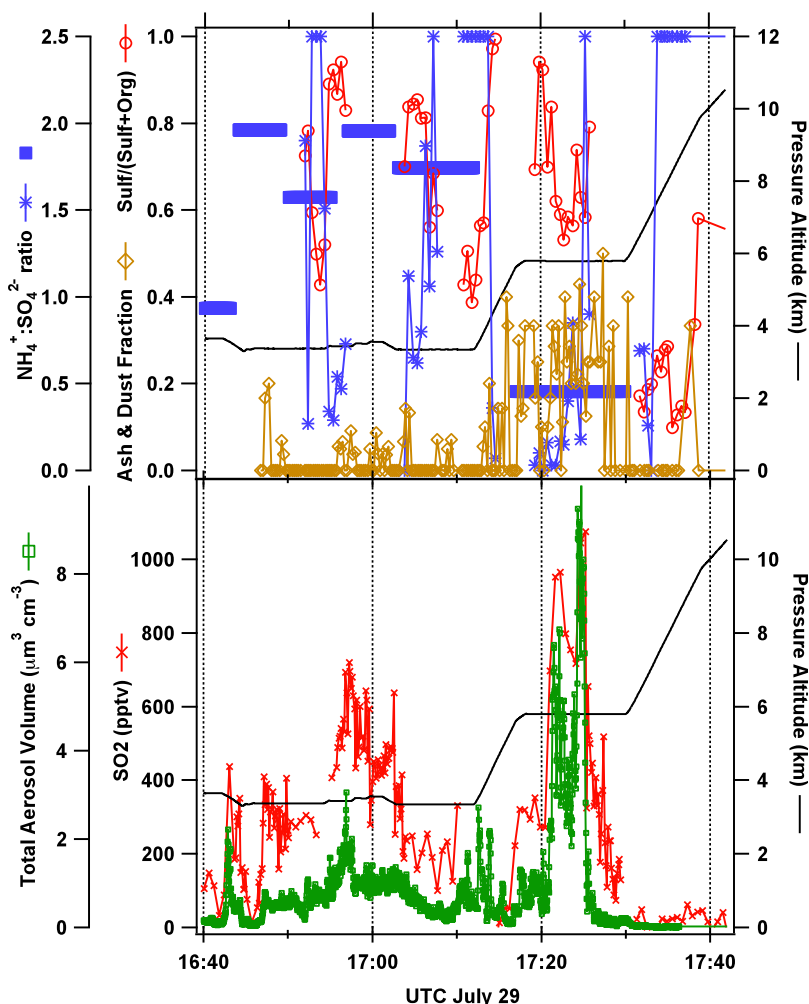
Figure 10. (top) PALMS single particle (open symbols) and SAGA bulk aerosol composition (solid squares) data and (bottom) LARGE aerosol volume and CIMS SO_2 mixing ratios for the 29 July volcanic plume penetration. The abscissa shows UTC time, and the black line indicates the aircraft altitude. The plume sampled at 1654–1704 UTC has little in the way of ash enhancement, consistent with a limited increase in total aerosol volume. The higher-level plume sampled at 1712–1730 UTC has more PALMS ash signatures and higher coarse mode aerosol volume. Relative sulfate/organic ratio (sulf/(sulf + org) in Figure 10 (top) indicates how sulfate-rich the nonrefractory accumulation mode aerosols are. The data show periods with very sulfate-rich particles, presumably as a result of H_2SO_4 condensation from volcanic SO_2, but the locations do not always correlate with high SO_2. The sulfate-rich particles are highly acidic (low $NH_4^+:SO_4^{2-}$ ratios). PALMS $NH_4^+:SO_4^{2-}$ data agree fairly well with bulk SAGA $NH_4^+:SO_4^{2-}$ values. Aerosol volume and SO_2 enhancements seem well correlated.

CO_2, CO and NO_2 (not shown) increase in direct proportion to CWC and O_3 shows a slight increase (Figure 13). The longer SAGA sampling interval precludes any observations of rapid variations in sulfate concentrations. Enhanced in-cloud mixing ratios of CO_2, CO and NO_2 (relative to ambient values) could result from the concentration of these relatively insoluble species in interstitial air (Henry's Law coefficients in M atm^{-1} for liquid water at 298 K are, CO: ~1×10^{-3}; NO_2: 1×10^{-2}; O_3: 1.1×10^{-2}; CO_2: 3.4×10^{-2}; SO_2: 1.23; H_2O_2: 1×10^5 (note that some of these coefficients are pH-dependent)) [*Seinfeld and Pandis*, 2006].

[45] Several competing processes may influence in-cloud concentrations of O_3 including aqueous-phase chemistry and photochemical reactions [e.g., *Thompson*, 1984; *Lelieveld and Crutzen*, 1990; *Acker et al.*, 1995; *Wang and Sassen*, 2000]. The observed minor increase in O_3 may result from the interplay of solubility-induced enrichment and photochemical O_3 depletion. Rates of O_3 loss via photodissociation should be more rapid at the cloud top, which could explain why a spike in O_3 is only seen in the lower-altitude portion of the cloud (Figure 13). *Crawford et al.* [2003] also found elevated CO and other anthropogenic trace gases in clouds over the Pacific during the TRACE-P experiment, but no clear difference in O_3 between clear and cloudy regions.

[46] It appears that H_2O_2, rather than O_3, was the main SO_2 oxidant during cloud processing of the Huila volcanic plume. Aqueous-phase oxidation of SO_2 by O_3 in clouds depends on the pH of the cloud water. For an O_3 concentration of 30 ppb, the rate constant for oxidation of S(IV) to S(VI) by O_3 decreases by 6 orders of magnitude as the pH reduces
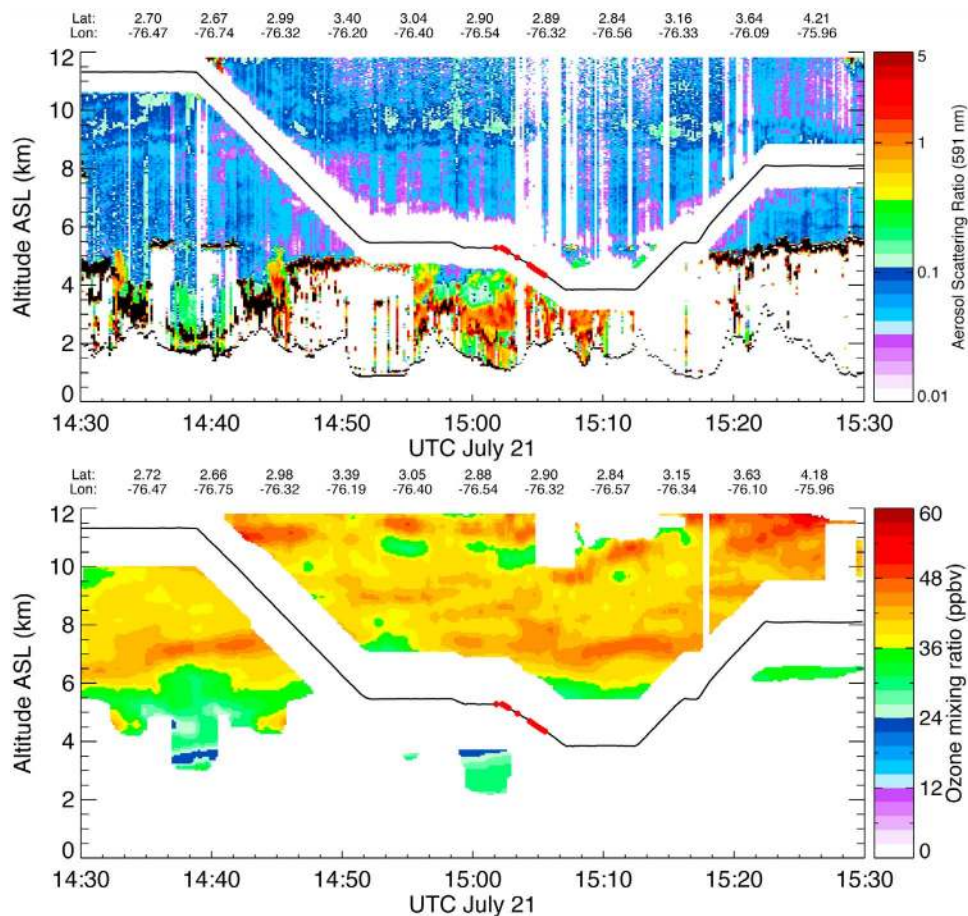
Figure 11. DIAL profiles of (top) ASR$_{VS}$ (591 nm) and (bottom) ozone mixing ratio on 21 July, 1430–1530 UTC (DC-8 flight 6). The black line indicates the aircraft altitude, and red segments indicate where SO$_2 \geq 0.5$ ppbv was measured by CIMS. Geographic coordinates of selected waypoints are plotted above the profiles. Note lidar returns from the Colombian topography. A zone of elevated O$_3$ concentrations measured at ~1433 and 1445 UTC and 4–5 km altitude is the Huila SO$_2$ plume.

from 6 to 1 [*Seinfeld and Pandis*, 2006], whereas oxidation by H$_2$O$_2$ is relatively insensitive to pH [*Eatough et al.*, 1994]. The pH of water in a cloud mixing with a volcanic plume would be low, favoring reaction with H$_2$O$_2$. H$_2$O$_2$ abundance is mainly determined by mixing ratios of O$_3$, CO, NO$_x$, and H$_2$O, and by the intensity of UV radiation, with the main sinks being heterogeneous loss (wet and dry deposition), liquid phase conversion, homogeneous gas phase oxidation by OH, and photolysis [*Jacob and Klockow*, 1992]. Global tropospheric chemistry models predict H$_2$O$_2$ mixing ratios between a few pptv to ~5 ppbv as a function of latitude, altitude, and season, with the highest values in equatorial regions during summer [*Jacob and Klockow*, 1992], so elevated H$_2$O$_2$ mixing ratios would be expected in the equatorial Ecuador/Colombia region in July, particularly at high altitudes. Up to 1.3 ppbv H$_2$O$_2$ was measured from the DC-8 near Huila on 21 July, and up to 4 ppbv was detected on 17 July in the Ecuadorian outflow, indicating that supply of H$_2$O$_2$ in the region is not limited. Furthermore, H$_2$O$_2$ was also enhanced within the Huila plume (~0.5 ppbv; Figure 13). A possible origin of elevated H$_2$O$_2$ is self-reaction of HO$_2$ radicals in the young plume, with HO$_2$ initially generated by high-temperature

chemistry in the very fresh, water-rich mixture [*Roberts et al.*, 2009]:

$$HO_2 + HO_2 \rightarrow H_2O_2 + O_2 \qquad (1)$$
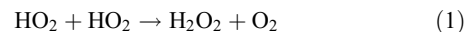
Modeling suggests that production of ~10 ppbv of H$_2$O$_2$ is possible via this reaction, which then rapidly decreases and stabilizes. In summary, while the role of H$_2$O$_2$ in aqueous-phase SO$_2$ oxidation is well known in the context of anthropogenic plumes, the TC⁴ data may provide the first comprehensive in situ observations of cloud processing in a tropospheric volcanic plume involving H$_2$O$_2$. Furthermore, the measurements support model predictions that the volcanic plume may itself provide a source of H$_2$O$_2$.

7. OMI SO$_2$ Validation

[47] Evaluation of trace gas retrievals from various spaceborne instruments was a major goal of TC⁴. Volcanic SO$_2$ plumes in Ecuador and Colombia are frequently observed by OMI [*Carn et al.*, 2008], and hence the campaign provided a rare opportunity to validate SO$_2$ columns retrieved by the operational OMI SO$_2$ algorithm [*Yang et al.*, 2007] in lower tropospheric volcanic emissions.
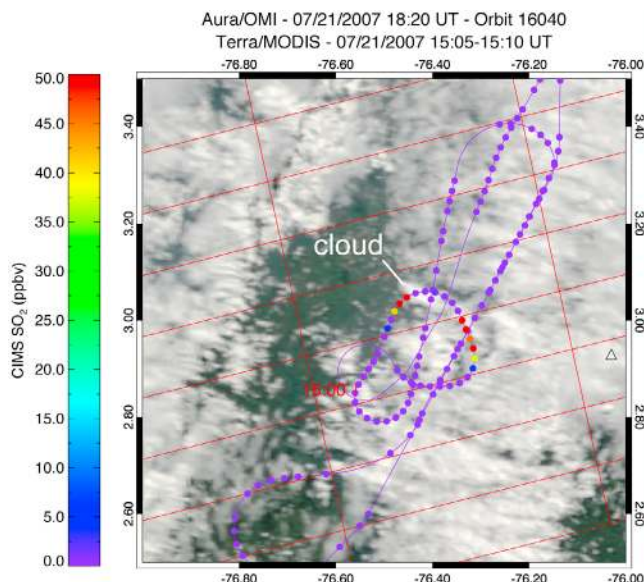
Figure 12. SO_2 mixing ratios measured by CIMS (circular symbols) during the DC-8 flight west of cloud-covered Huila volcano (triangle) on 21 July at ~1500 UT, superimposed on Terra/MODIS data collected at 1505–1510 UT. The meteorological cloud discussed in the text (section 6.2) is indicated. OMI ground-pixel boundaries for the 1820 UT Aura overpass are shown in red.

lower tropospheric (TRL) SO_2 product, which uses an a priori SO_2 plume center of mass altitude (CMA) of ~3 km. This a priori CMA is closest to the observed SO_2 vertical distribution in the Ecuadorian volcanic outflow, in which the peak SO_2 vmr was observed at ~4 km altitude (Table 2). Inspection of averaging kernels for the OMI TRL SO_2 retrieval indicates that the small difference between the a priori and actual SO_2 plume CMA in this case would result in a ~10%–20% overestimate of the SO_2 vertical column. The TRL SO_2 retrieval noise in a single OMI IFOV amounts to ~0.7 Dobson units (DU) (1σ) under optimal observational conditions in the tropics. Observational conditions in the
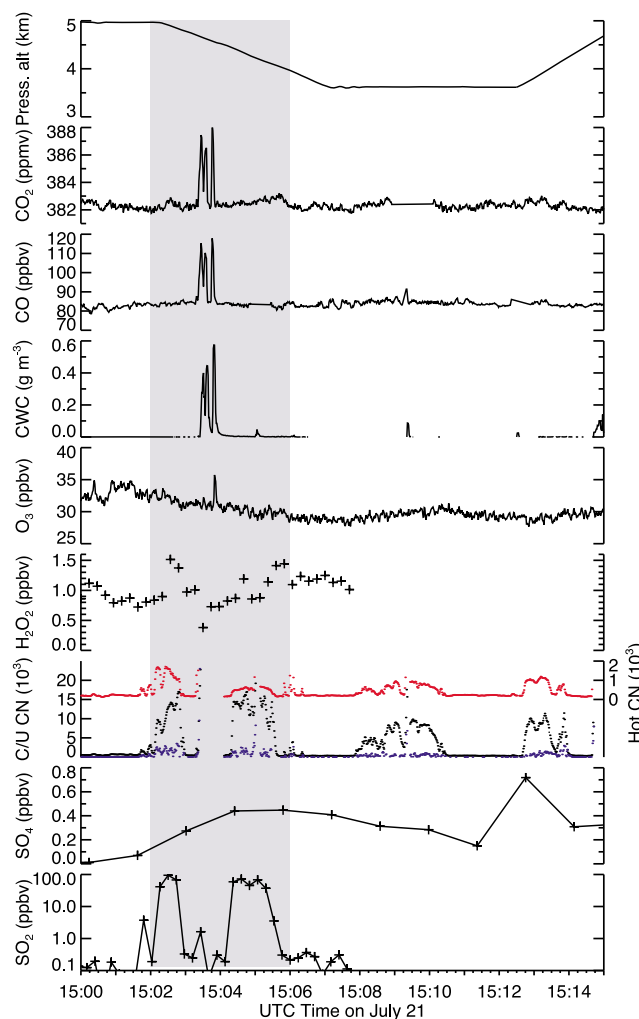
Figure 13. In situ measurements for volcanic plume penetrations on 21 July. From top to bottom, the parameters shown are DC-8 pressure altitude, CO_2 vmr, CO vmr, condensed water content (CWC), O_3 vmr, H_2O_2 vmr, condensation nuclei (CN) number density (subdivided into cold (C; black), hot (red), and ultrafine (U; blue)), aerosol SO_4^{2-} vmr, and SO_2 vmr (log scale). Note that these are discrete measurements with variable sampling intervals and integration times; some data points have been connected for clarity, but this does not imply continuous data. SO_2 and H_2O_2 were not measured from 1508–1515 UTC. Shaded region indicates plume 5 referred to in Table 2.

Spinei et al. [2010] report on a recent successful effort to validate OMI measurements of upper tropospheric and stratospheric SO_2 columns. Although the goal of sampling proximal emissions from Tungurahua was not achieved due to air traffic control restrictions in Ecuadorian airspace, the TC⁴ in situ data provide some valuable constraints on the vertical distribution of SO_2 in volcanic outflow regions.

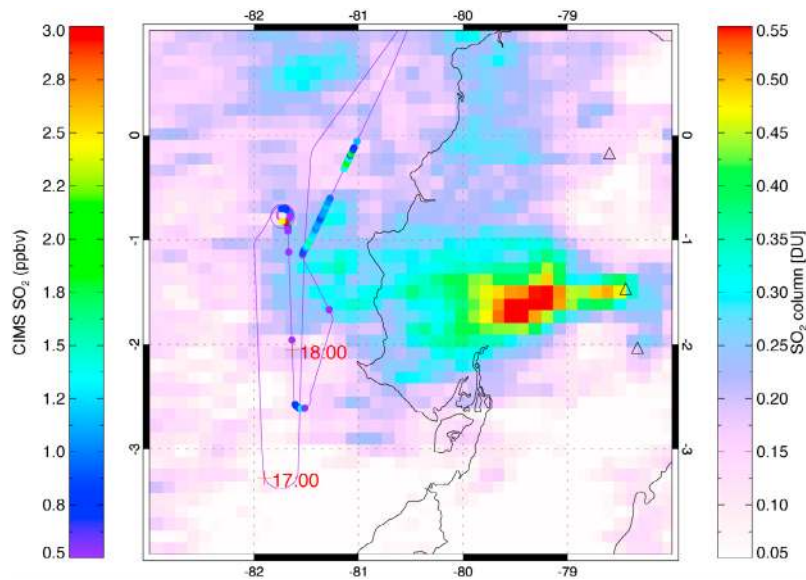### 7.1. The Tungurahua Volcanic Plume

[48] The 17 July flight west of Ecuador produced the smallest time difference between volcanic plume penetration by the DC-8 (plumes 3 and 4 at 1823–1837 UTC; Table 2 and Figure 5) and the Aura satellite overpass (1843–1844 UTC). The descending spiral through the volcanic outflow at 1730–1736 UTC (Figure 4), followed by the ascent through the plume at 1823–1837 UT, provide a vertical SO_2 profile that can be integrated to obtain a total column amount (following conversion of SO_2 mixing ratios to concentrations using air temperature and pressure measured in situ). Based on DIAL profiles (Figure 3), the top of the widespread stratus cloud deck visible in coincident MODIS data (Figure 4) was below ~2 km altitude, so we assume that this would not affect OMI measurements of the volcanic SO_2. However, these clouds would likely prevent space-based detection of any SO_2 in the marine PBL (e.g., ship plumes or SO_2 produced from oxidation of marine DMS), and so we excluded this from the total column integration.

[49] Operational SO_2 retrievals using OMI UV radiances require an a priori assumption of the vertical SO_2 distribution [*Yang et al.*, 2007], which is currently addressed by providing retrieved SO_2 columns corresponding to four different a priori SO_2 profiles. For this analysis we use the

Figure 14. SO$_2$ mixing ratios measured by CIMS (circular symbols, plotted only for SO$_2$ vmr ≥ 0.5 ppbv along the DC-8 flight track) during the DC-8 flight on 17 July, superimposed on a map of average SO$_2$ column amounts measured by OMI over the period 10–17 July 2007. The operational OMI lower tropospheric (TRL) SO$_2$ product was used for this analysis. OMI measurements suggest that Tungurahua was the main source of SO$_2$ west of Ecuador during this period.

Ecuador region (tropical, low total column O$_3$, low solar zenith angle) are close to optimal in this case.

[50] Integration of the in situ SO$_2$ vertical profile measured in the Ecuadorian volcanic outflow produces a maximum total SO$_2$ column of 0.095 DU (including PBL SO$_2$ results in a total column of 0.17 DU). This is considerably lower than the 1σ noise in the TRL data, and indeed no significant SO$_2$ column amounts (at the 3σ confidence level) were measured by OMI in the region of the DC-8 plume penetration during the 1843–1844 UTC overpass on 17 July, although a SO$_2$ plume from Tungurahua was detected further east over Ecuador. The SO$_2$ amounts measured during TC[4] are therefore too low to permit validation of OMI SO$_2$ measurements in the distal Tungurahua plume for a single OMI IFOV. However, calculation of a temporal average of OMI TRL SO$_2$ data for the 10–17 July 2007 period reveals the average SO$_2$ columns measured by OMI in the Ecuadorian volcanic outflow region, which show the predominant westward dispersion of the volcanic plume (Figure 14). The time-averaged OMI data still contains noise, and systematic errors (biases) in the SO$_2$ retrieval (such as those associated with meteorological clouds) [*Yang et al.*, 2007] can be exacerbated by averaging. However, the spatial coherence of the SO$_2$ signal extending west of Tungurahua in Figure 14 provides confidence that this is volcanic SO$_2$. We find that the in situ SO$_2$ column measured on 17 July is in agreement with average SO$_2$ columns of 0.2–0.4 DU measured by OMI in the distal Tungurahua plume during the preceding week. Thus, while validation of SO$_2$ measurements in a single OMI IFOV is not possible, the TC[4] data are consistent with the time-averaged OMI SO$_2$ measurements.

7.2. The Huila Volcanic Plume

[51] OMI measurements on 21 July at 1820 UTC show a SO$_2$ plume extending ~WNW of Huila. Although the SO$_2$

amounts sampled in situ in the Huila plume on 21 July were 1–2 orders of magnitude higher than those measured west of Ecuador, comparison between the TC[4] data and OMI SO$_2$ measurements in this case is compromised by several factors. First, the 1820 UTC Aura overpass of Huila on 21 July occurred over 3 h after collection of the in situ SO$_2$ data, and consideration of the dynamic nature of typical volcanic emissions suggests that significant spatial and compositional changes in the SO$_2$ plume are likely on such timescales. Furthermore, as noted previously, significant convective cloud development occurred between the DC-8 plume penetration at ~1500 UTC (Figure 12) and the Aura overpass, which would have affected SO$_2$ concentrations (based on our observations of in-cloud SO$_2$ depletion; section 6.2) and would also impact the satellite measurement sensitivity through modification of the air mass factor (AMF). Another complication is that the DC-8 did not sample the entire vertical extent of the Huila plume, so interpolation is necessary to yield a continuous vertical SO$_2$ profile. Finally, the region of interest coincided with off-nadir OMI viewing angles on 21 July, producing relatively large footprint sizes (Figure 12). Spatial averaging of plume SO$_2$ over the area of an OMI pixel must therefore be taken into account, but is hard to constrain owing to a lack of information on the physical dimensions of the plume.

[52] Given these limitations, we only attempt a preliminary comparison here. By interpolating SO$_2$ mixing ratios across the data gap induced by the meteorological cloud (Figure 13), we obtain an estimate of the vertical SO$_2$ profile for the Huila plume. The SO$_2$ column content of this profile is ~3 DU, with a plume CMA of 4.6 km. The OMI TRL SO$_2$ column in the pixel west of Huila (centered at 2.96°N, 76.38°W) is 0.92 DU, and the retrieval averaging kernel suggests a ~30% overestimate of the SO$_2$ column for a plume at 4.6 km altitude, giving an adjusted SO$_2$ column of
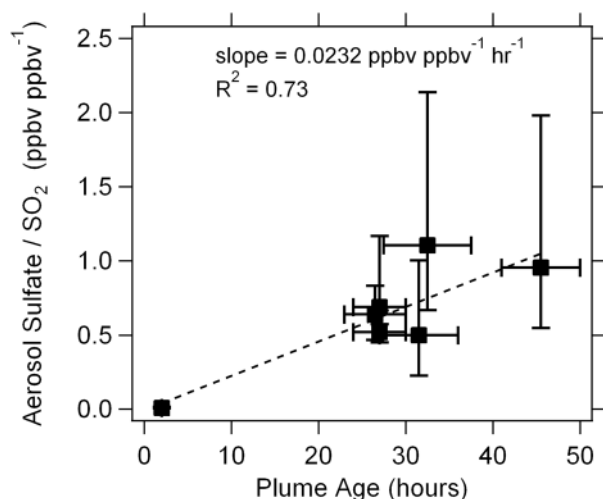
Figure 15. Aerosol SO_4^{2-}:SO_2 ratio against plume age for the TC[4] volcanic plume data. Aerosol SO_4^{2-} is from the SAGA experiment, and SO_2 is from CIMS (Table 1). Data points are median values of the sulfate ratio, and error bars represent quartile ranges. Plume ages are from the HYSPLIT back-trajectory analysis (section 4; assuming no contributions from Reventador), with horizontal error bars showing the range of plume age estimates.

0.64 DU. The difference between the in situ and OMI SO_2 columns can be at least partly ascribed to averaging over the ~ 840 km^2 area covered by the OMI pixel. Assuming Gaussian dispersion of a point-source plume emanating from Huila volcano, with plume edges constrained by the in situ SO_2 measurements, we arrive at an estimated plume area of ~ 275 km^2 within the OMI pixel. Hence spatial averaging would produce a $\sim$three-fold dilution of the actual SO_2 column in this case, i.e., ~ 1 DU. This is of a similar magnitude to the OMI SO_2 retrieval (the difference could be explained by increased in-cloud SO_2 depletion in the plume prior to the OMI overpass), but cannot be considered validation due to the uncertainties listed above. In particular, a rigorous treatment of the problem requires radiative transfer calculations to model the local AMF, which critically depends on the vertical profile, altitude and spatial scale of the meteorological clouds present at the time of the OMI measurements, which are poorly constrained.

8. Discussion

[53] The TC[4] measurements are a valuable contribution to the existing, limited data on in situ volcanic plume composition. The age range of the Ecuadorian plumes sampled during TC[4] (>24 h in some cases) sets them apart from most previous direct sampling studies. In situ measurements of O_3 within volcanic plumes using the chemiluminescence technique (also used by *Hobbs et al.* [1982]), which is not susceptible to interference by SO_2, are also rare [*von Glasow*, 2010]. Particle number densities encountered in the Tungurahua and Huila volcanic plumes are 1–2 orders of magnitude lower than those measured in proximal (~ 20 km downwind) emissions from volcanoes exhibiting more vigorous eruptive activity, such as Redoubt (Alaska) in January 1990 [*Hobbs et al.*, 1991]. Particle diameter modes

observed in the TC[4] volcanic plumes are broadly similar to existing data (see *Mather et al.* [2003a] for a compilation), with peaks in the accumulation and/or coarse particle modes, depending on the style of volcanic activity and the sampling location relative to the vent. Although the TC[4] plume penetrations were brief and particle counts were low, there are several noteworthy aspects of the data set that we highlight here.

8.1. Sulfur Chemistry and Plume Aging

[54] Given the significant contribution of volcanic emissions to the global tropospheric sulfate budget [e.g., *Graf et al.*, 1997], it is worthwhile to discuss SO_2-to-sulfate conversion in the light of the TC[4] observations of aged plumes. SO_2 oxidation may proceed via gas phase (e.g., reaction with OH), aqueous phase (e.g., oxidation by H_2O_2 or O_3), or particle surface reactions [e.g., *Eatough et al.*, 1984, 1994; *Mather et al.*, 2003b; *Seinfeld and Pandis*, 2006]. The reaction is complex, owing to the influence of variable factors such as irradiation, humidity, oxidant abundance and the presence of catalysts (e.g., metals) [*Mather et al.*, 2003b]. *Möller* [1980] derived average first-order reaction rates (k_1) for background tropospheric oxidation of SO_2 according to [*Mather et al.*, 2003b]

$$(SO_2)_t = D(SO_2)_0 \exp(-k_1 t) \tag{2}$$

where $(SO_2)_t$ is the SO_2 concentration at time t, $(SO_2)_0$ is the initial SO_2 concentration, and D is a dilution coefficient. *Möller* [1980] found k_1 values (in s^{-1}) of 1.2×10^{-6}, $\geq 5 \times 10^{-5}$, and $(0.1–10) \times 10^{-5}$ for gas phase, aqueous phase, and particle surface reactions, respectively. *Eatough et al.* [1994] found that k_1 could vary from $<1\%$ h^{-1} (gas phase) to $>500\%$ h^{-1} (aqueous phase) in anthropogenic SO_2 emissions, depending on meteorological conditions and particle microphysics. A similarly wide range of SO_2 depletion rates has been reported from studies of tropospheric volcanic plumes [e.g., *Oppenheimer et al.*, 1998; *Porter et al.*, 2002; *Satsumabayashi et al.*, 2004; *McGonigle et al.*, 2004; *Rodríguez et al.*, 2008; *Oppenheimer et al.*, 2010].

[55] The TC[4] data do not include upwind and downwind measurements of the same volcanic plume, precluding a direct calculation of the SO_2 loss rate. For the cloud-processed Huila plume (Figure 13), we can assume an initial SO_2 mixing ratio of at least 100 ppbv, with 1 ppbv SO_2 remaining after ~ 2 h of plume transport, and use (1) to constrain k_1 to be $\geq 6 \times 10^{-4}$ s^{-1} ($\sim 230\%$ h^{-1}; ignoring dilution); consistent with reported aqueous phase reaction rates. Amalgamating all the TC[4] plume SO_2 and sulfate aerosol data (Figure 15) allows us to draw some general conclusions on SO_2-to-aerosol conversion in the volcanic outflow region. Despite the fact that the data represent a mixture of volcanic sources and emission times, Figure 15 suggests that aerosol sulfate production follows an upward trend. Using fine mode aerosol volume, rather than aerosol sulfate, as the numerator on the ordinate does not produce the same trend due to varying amounts of fine mode volcanic ash and organic material mixed in. The trend in Figure 15 is equivalent to an average SO_2 to sulfate conversion rate of $\sim 1\%$–2% h^{-1}, again assuming first-order kinetics, consistent with previously reported rates for gas phase reactions [e.g., *Möller*, 1980]. We therefore conclude

that any volcanic SO_2 emitted in the region that eludes cloud processing will have a relatively long lifetime in the Pacific midtroposphere, probably due in part to the high altitude of the Ecuadorian and Colombian volcanoes. Extended production of fine-mode sulfate aerosol via gas-to-particle conversion in the volcanic plumes is significant, since such particles are small and have long atmospheric residence times, promoting long-range transport.

[56] Aerosol bulk composition data from the SAGA experiment generally show a good correlation between SO_4^{2-} and NH_4^+ for all TC[4] data suggesting neutralization of H_2SO_4 by NH_3 to various degrees. The volcanic plume aerosol data are limited but generally consistent, though with evidence for sulfate enrichment (perhaps indicating exhaustion of NH_3) on 17 July (1824–1836 UT) and 29 July (1712–1730 UT). It should be noted that these data are limited and do not include all the volcanic plumes sampled.

[57] The phase and composition of volcanic sulfate particles impacts their optical properties and hence climate forcing. Neutralization of sulfuric acid to form solid particles in the middle-to-upper troposphere is therefore a key process. Aircraft data show that sulfate at high altitudes (>5 km) is usually highly neutralized [e.g., *Dibb et al.*, 2003a, 2003b]. The availability of NH_3 for neutralization of sulfate has been attributed to the low retention efficiency of NH_3 in ice, such that NH_3 in water cloud droplets is released at high altitudes upon freezing [*Wang et al.*, 2008].

[58] Consistent with the SO_2-to-sulfate conversion conclusions above, the Ecuadorian volcanic plumes sampled on 17 and 29 July both show a 0.1 μm diameter mode (condensation submode) in their aerosol spectra, but this mode is absent in the Huila spectra (Figure 7). All plumes, however, show a 0.5–0.6 μm accumulation mode (Figure 7). The Huila aerosol spectra also indicate the presence of Aitken mode particles (~0.05–0.06 μm). The 0.5 μm mode represents both sulfate-coated ash grains as well as pure sulfate particles, possibly a result of cloud processing. The 0.1 μm mode is probably derived from direct gas-to-particle condensation. The absence of the 0.1 μm mode in the Huila plume may reflect a freshly cloud-processed plume, in which the 0.1 μm mode has not yet been reestablished by vapor condensation and particle coagulation.

8.2. Ozone and NO_y Chemistry

[59] Coincident with the peak in SO_2 vmr in the Ecuadorian plume at 1731–1732 UTC on 17 July (Figure 5), we note a small increase in HNO_3 (~80–90 pptv) and a decrease in O_3 (~8 ppbv; ~20% of ambient levels). At lower altitudes during this plume penetration, HNO_3 and sulfate concentrations increase (peaking at ~0.2 and 0.6 ppbv, respectively), as does the SO_4^{2-}:SO_2 ratio, indicating an aged plume or one that has undergone cloud processing. A ~12 ppbv reduction in O_3 (~30% of ambient levels) and ~75 pptv increase in HNO_3 are also associated with the SO_2 peak measured at 1833 UTC on 17 July (Figure 5), along with a similar increase in HNO_3 and sulfate at lower altitudes. In both cases the HNO_3 and sulfate maxima in the vicinity of the volcanic plume are collocated. Similar relationships are not apparent in the 29 July data (Figure 6), though in this case the plume may have been entrained in Amazonian outflow, impacting the O_3 mixing ratios. Independent HNO_3 measurements by three DC-8 instruments

(CIMS, SAGA and TD-LIF, each with different integration times; Table 1) give similar results.

[60] In-plume chemical depletion of O_3 has been invoked at a handful of volcanoes, but not yet in a tropospheric volcanic plume of an age similar to the 17 July Ecuadorian plumes. *Fruchter et al.* [1980] found O_3 reduced by ~33% relative to ambient levels 200 km downwind of Mt St Helens in May 1980. As noted by *Oppenheimer et al.* [2010], who report O_3 depletion in the plume from Erebus volcano (Antarctica), direct evidence for in-plume O_3 loss in tropospheric volcanic plumes is sparse [*Stith et al.*, 1978; *Fruchter et al.*, 1980; *Hobbs et al.*, 1982]. Since the first identification of BrO in a tropospheric volcanic plume [*Bobrowski et al.*, 2003], considerable attention has been devoted to reactive halogen chemistry in volcanic emissions and its potential impact on O_3 [e.g., *Gerlach*, 2004; *Oppenheimer et al.*, 2006; *Bobrowski et al.*, 2007; *Roberts et al.*, 2009]. Numerical modeling by *von Glasow* [2010] suggests that O_3 depletion could be maintained for >70 h after plume release, but the author also stresses the importance of plume mixing, which can be complex. Reactive chlorine chemistry involving the formation of ClO and OClO, which may predominate after depletion of HBr in the plume, also merits further consideration. Modeling indicates that ClO and OClO concentrations continue to increase up to the 60 min runtime used by *Roberts et al.* [2009], although they also note the uncertainty in our understanding of reactive chlorine chemistry in volcanic plumes.

[61] We believe the TC[4] data alone are insufficient to ascribe the observed O_3 concentrations to chemical depletion of O_3 in the Ecuadorian volcanic plumes. We looked for evidence of heterogeneous reactive halogen chemistry in PALMS data, which can detect reactive halogens partitioned to aerosol. The 17 July plume particles showed no obvious enhancements in Br, Cl or I, except possible evidence for enhanced Br in plume 7 on 29 July. An equally plausible explanation for the O_3 observations is that air entrained into the volcanic plume was advected into a region with slightly higher O_3 concentrations (note that O_3 concentrations typically increase with altitude, e.g., Figure 5), giving the impression of in-plume O_3 loss. In-plume O_3 concentrations on 17 July could also be impacted by its role in SO_2 oxidation. The reaction rate for aqueous-phase SO_2 oxidation by O_3 increases with pH [*Seinfeld and Pandis*, 2006], so as sulfate is produced by the reaction, the reaction slows down. In situ O_3 concentrations in ambient air at the source would be needed to clarify the fate of O_3 entrained into the volcanic plume.

[62] Significantly, we also observe no evidence for O_3 depletion in the Huila plume, sampled ~2 h downwind of the vent, despite the fact that it contained ~100 ppbv of SO_2 and high particle concentrations to support heterogeneous reactions (Figure 13). This could reflect insufficient concentrations of HBr in the plume to sustain the autocatalytic BrO reaction cycle that consumes O_3, or perhaps simply that any near-source O_3 depletion had been replenished through mixing with ambient air by the sampling time. Modeling by *Roberts et al.* [2009] shows in-plume O_3 mixing ratios recovering to ~70% of initial ambient levels (a value of 64 ppbv was used) after 60 min. This is due to exhaustion of HBr during plume dispersion, which removes the source of reactive Br. In contrast to the 17 July measurements, the

O_3 concentrations measured in the vicinity of the Huila plume are more likely to reflect those at the source, arguing against any significant in-plume O_3 processing.

[63] Elevated HNO_3 concentrations have been observed previously in volcanic plumes, but their origin remains unclear. Volcanic HNO_3 concentrations of 200 ppbv above background have been measured on the crater rim of Masaya, with elevated HNO_3 also noted in other proximal volcanic plumes (Etna, Lascar and Villarrica) [*Mather et al.*, 2004a, 2004b], but other studies at Masaya and elsewhere have detected no near-source HNO_3 [*Lazrus et al.*, 1979; *Martin et al.*, 2010]. The coupled NO_y and reactive halogen chemistry simulated by *Roberts et al.* [2009] is consistent with elevated HNO_3 in some young volcanic plumes and with limited observations of in-plume O_3 depletion [*Lee et al.*, 2005; *Oppenheimer et al.*, 2010]. *Roberts et al.* [2009] only simulate plume chemistry during the first hour of transport, noting that O_3 depletion reaches 20–60% after 60 min, although further O_3 depletion is expected downwind [e.g., *von Glasow*, 2010]. Importantly however, the reaction scheme requires plume NO_x, which is assumed to originate from high-temperature nitrogen fixation close to the volcanic vent. We consider high levels of NO_x unlikely in the Tungurahua and Huila volcanic emissions owing to the style of volcanic activity. In situ TC^4 data show that NO_2 was not obviously elevated in the young Huila plume (and NO measurements using TC^4 were limited), although HNO_3 (not shown) was above ambient levels (~100 pptv against a background of ~50 pptv), perhaps suggesting oxidation of plume NO_x during transport.

[64] Displacement from acidified background and/or volcanic aerosol [e.g., *Allen et al.*, 2002; *Mather et al.*, 2004b] may therefore be the most likely source of elevated HNO_3 in the Ecuadorian volcanic outflow. This would be consistent with the collocated peaks in HNO_3 and sulfate mixing ratios. Observations of peaks in HNO_3 and SO_4^{2-} beneath the SO_2 peak (e.g., Figure 5) could be interpreted as evidence of gravitational separation of the aerosol and gas phases in the Ecuadorian plumes. Observations 12–18 h downwind of Miyakejima lead *Satsumabayashi et al.* [2004] to propose that, with progressive acidification, sulfate first exhausts NH_3 to form $(NH_4)_2SO_4$ aerosol, and then expels NO_3^- and Cl^- (acidifying the aerosol). This process sometimes formed pure sulfuric acid mist after titration of NH_3, and exacerbated wet deposition of HNO_3 and HCl and hence environmental acidification [*Satsumabayashi et al.*, 2004].

9. Conclusions

[65] Previous efforts to sample volcanic plumes in situ include the pioneering aircraft sampling campaigns of the 1970s and 1980s, and more recent measurements made on the crater rims of volcanoes, such as Etna and Masaya, with accessible vent regions fumigated by volcanic emissions. The TC^4 data set discussed here offers a rare window into the composition of aged volcanic plumes sampled in situ in the tropical Pacific troposphere.

[66] The TC^4 measurements provide further insight into the composition and evolution of tropospheric volcanic plumes. Accumulation mode aerosol sampled in Ecuadorian volcanic outflow was highly acidic, and such particles are a significant health hazard owing to their long atmospheric

residence times and ability to penetrate into the lung [e.g., *Mather et al.*, 2003a; *Longo et al.*, 2005]. The Huila plume penetrations show the effects of near-source cloud processing involving H_2O_2 on SO_2 concentrations in tropical volcanic plumes. This processing undoubtedly has a significant effect on SO_2 abundance in volcanic plumes in the tropics, impacting SO_2 emission rate measurements in cloudy or partly cloudy regions.

[67] The TC^4 data also suggest that volcanic SO_2 emissions from the Ecuadorian and Colombian cordilleras that are not cloud processed have relatively long lifetimes, perhaps due to a predominance of homogeneous gas phase oxidation, and are a source of fine-mode sulfate aerosol far downwind. SO_2 and sulfate levels measured in volcanic plumes over 300 km from the source during TC^4 are more than an order of magnitude higher than levels measured at the same altitude in the remote central and tropical Pacific troposphere by *Thornton et al.* [1996]. The volcanogenic sulfate aerosol must therefore represent an important source of CN in the tropical midtroposphere, with possible radiative cooling effects. The persistence of coarse mode ash particles in the 29 July plume may have significant ramifications for heterogeneous chemistry in volcanic plumes (e.g., involving reactive halogens).

[68] The SO_2 concentrations encountered during TC^4 were not sufficient to provide a robust validation of OMI SO_2 measurements in the volcanic plumes. However, we find consistency between the in situ SO_2 concentrations and profiles and average SO_2 column amounts retrieved from OMI measurements during the experiment. A better validation data set would require in situ measurements much closer to the source volcano and/or during periods of higher SO_2 emissions.

[69] In-plume O_3 concentrations ~20%–30% below ambient levels were observed in Ecuadorian volcanic outflow, but no perturbation of in-plume O_3 levels was observed in the younger Huila plume. Based on the TC^4 data alone, the most likely cause of low in-plume O_3 is advection of a plume with low O_3 inherited from the source region into an air mass with higher ambient O_3 concentrations, although reactive halogen chemistry merits further examination.

References

Acker, K., W. Wieprecht, D. Möller, G. Mauersberger, S. Naumann, and A. Oestreich (1995), Evidence of ozone destruction in clouds, *Naturwissenschaften*, *82*, 86–89, doi:10.1007/BF01140147.

Allard, P., et al. (1991), Eruptive and diffuse emissions of CO_2 from Mount Etna, *Nature*, *351*, 387–391, doi:10.1038/351387a0.

Allen, A. G., C. Oppenheimer, M. Ferm, P. J. Baxter, L. A. Horrocks, B. Galle, A. J. S. McGonigle, and H. J. Duffell (2002), Primary sulfate aerosol and associated emissions from Masaya Volcano, Nicaragua, *J. Geophys. Res.*, *107*(D23), 4682, doi:10.1029/2002JD002120.

Andreae, M. O., and T. W. Andreae (1988), The cycle of biogenic sulfur compounds over the Amazon Basin: 1. Dry season, *J. Geophys. Res.*, *93*, 1487–1497, doi:10.1029/JD093iD02p01487.

Andres, R. J., and A. D. Kasgnoc (1998), A time-averaged inventory of subaerial volcanic sulfur emissions, *J. Geophys. Res.*, *103*, 25,251–25,261, doi:10.1029/98JD02091.

Arellano, S. R., M. Hall, P. Samaniego, J.-L. Le Pennec, A. Ruiz, I. Molina, and H. Yepes (2008), Degassing patterns of Tungurahua volcano (Ecuador) during the 1999–2006 eruptive period, inferred from remote spectroscopic measurements of SO$_2$ emissions, *J. Volcanol. Geotherm. Res.*, *176*(1), 151–162, doi:10.1016/j.jvolgeores.2008.07.007.

Baxter, P. J., R. E. Stoiber, and S. N. Williams (1982), Volcanic gases and health: Masaya volcano, Nicaragua, *Lancet*, *320*, 150–151, doi:10.1016/S0140-6736(82)91109-6.

Bobrowski, N., G. Hönninger, B. Galle, and U. Platt (2003), Detection of bromine monoxide in a volcanic plume, *Nature*, *423*, 273–276, doi:10.1038/nature01625.

Bobrowski, N., R. von Glasow, A. Aiuppa, S. Inguaggiato, I. Louban, O. W. Ibrahim, and U. Platt (2007), Reactive halogen chemistry in volcanic plumes, *J. Geophys. Res.*, *112*, D06311, doi:10.1029/2006JD007206.

Brazier, S., A. N. Davis, H. Sigurdsson, and R. S. J. Sparks (1982), Fallout and deposition of volcanic ash during the 1979 explosive eruption of the Soufriere of St. Vincent, *J. Volcanol. Geotherm. Res.*, *14*(3–4), 335–359, doi:10.1016/0377-0273(82)90069-5.

Browell, E. V., A. F. Carter, S. T. Shipley, R. J. Allen, C. F. Butler, M. N. Mayo, J. H. Siviter Jr., and W. M. Hall (1983), NASA multipurpose airborne DIAL system and measurements of ozone and aerosol profiles, *Appl. Opt.*, *22*(4), 522–534, doi:10.1364/AO.22.000522.

Browell, E. V., W. B. Grant, and S. Ismail (2005), Airborne lidar systems, in *Laser Remote Sensing*, *Opt. Eng.*, vol. 97, edited by T. Fujii and T. Fukuchi, pp. 723–780, CRC Press, Boca Raton, Fla.

Cadle, R. D., A. L. Lazrus, and J. P. Shedlovsky (1969), Comparison of particles in the fume from eruptions of Kilauea, Mayon, and Arenal volcanoes, *J. Geophys. Res.*, *74*, 3372–3378, doi:10.1029/JC074i013p03372.

Cadle, R. D., A. L. Lazrus, B. J. Huebert, L. E. Heidt, W. I. Rose Jr., D. C. Woods, R. L. Chuan, R. E. Stoiber, D. B. Smith, and R. A. Zielinski (1979), Atmospheric implications of studies of Central American volcanic eruption clouds, *J. Geophys. Res.*, *84*, 6961–6968, doi:10.1029/JC084iC11p06961.

Carn, S. A., A. J. Krueger, N. A. Krotkov, S. Arellano, and K. Yang (2008), Daily monitoring of Ecuadorian volcanic degassing from space, *J. Volcanol. Geotherm. Res.*, *176*(1), 141–150, doi:10.1016/j.jvolgeores.2008.01.029.

Casadevall, T. J., W. I. Rose Jr., W. H. Fuller, W. H. Hunt, M. A. Hart, J. L. Moyers, D. C. Woods, R. L. Chuan, and J. P. Friend (1984), Sulfur dioxide and particles in quiescent volcanic plumes from Poás, Arenal, and Colima volcanoes, Costa Rica and Mexico, *J. Geophys. Res.*, *89*, 9633–9641, doi:10.1029/JD089iD06p09633.

Chin, M., and D. Jacob (1996), Anthropogenic and natural contributions to tropospheric sulfate: A global model analysis, *J. Geophys. Res.*, *101*, 18,691–18,699.

Crawford, J., et al. (2003), Clouds and trace gas distributions during TRACE-P, *J. Geophys. Res.*, *108*(D21), 8818, doi:10.1029/2002JD003177.

Day, D. A., P. J. Wooldridge, M. B. Dillon, J. A. Thornton, and R. C. Cohen (2002), A thermal dissociation laser-induced fluorescence instrument for in situ detection of NO$_2$, peroxy nitrates, alkyl nitrates, and HNO$_3$, *J. Geophys. Res.*, *107*(D6), 4046, doi:10.1029/2001JD000779.

Delmelle, P. (2003), Environmental impacts of tropospheric volcanic gas plumes, in *Volcanism and the Earth's Atmosphere*, *Geophys. Monogr. Ser.*, vol. 139, edited by A. Robock and C. Oppenheimer, pp. 381–399, AGU, Washington, D. C.

Delmelle, P., M. Lambert, Y. Dufrene, P. Gerin, and N. Oskarsson (2007), Gas/aerosol-ash interaction in volcanic plumes: New insights from surface analysis of fine volcanic ash, *Earth Planet. Sci. Lett.*, *259*, 159–170, doi:10.1016/j.epsl.2007.04.052.

Dibb, J. E., R. W. Talbot, G. Seid, C. Jordan, E. Scheuer, E. Atlas, N. J. Blake, and D. R. Blake (2003a), Airborne sampling of aerosol particles: Comparison between surface sampling at Christmas Island and P-3 sampling during PEM-Tropics B, *J. Geophys. Res.*, *108*(D2), 8230, doi:10.1029/2001JD000408.

Dibb, J. E., R. W. Talbot, E. M. Scheuer, G. Seid, M. A. Avery, and H. B. Singh (2003b), Aerosol chemical composition in Asian continental outflow during the TRACE-P campaign: Comparison with PEM-West B, *J. Geophys. Res.*, *108*(D21), 8815, doi:10.1029/2002JD003111.

Duggen, S., P. Croot, U. Schacht, and L. Hoffmann (2007), Subduction zone volcanic ash can fertilize the surface ocean and stimulate phytoplankton growth: Evidence from biogeochemical experiments and satellite data, *Geophys. Res. Lett.*, *34*, L01612, doi:10.1029/2006GL027522.

Eatough, D. J., R. J. Arthur, N. L. Eatough, M. W. Hill, N. F. Mangelson, B. E. Richter, and L. D. Hansen (1984), Rapid conversion of SO$_2$(g) to sulfate in a fog bank, *Environ. Sci. Technol.*, *18*, 855–859, doi:10.1021/es00129a009.

Eatough, D. J., F. M. Caka, and R. J. Farber (1994), The conversion of SO$_2$ to sulfate in the atmosphere, *Isr. J. Chem.*, *34*(3–4), 301–314.

Fisher, R. V. (1964), Settling velocity of glass shards, *Deep Sea Res. Oceanogr. Abstr.*, *12*, 345–353.

Froyd, K. D., D. M. Murphy, T. J. Sanford, D. S. Thomson, J. C. Wilson, L. Pfister, and L. Lait (2009), Aerosol composition of the tropical upper troposphere, *Atmos. Chem. Phys.*, *9*, 4363–4385, doi:10.5194/acp-9-4363-2009.

Fruchter, J. S., et al. (1980), Mount St. Helens ash from the 18 May 1980 eruption: Chemical, physical, mineralogical and biological properties, *Science*, *209*, 1116–1125, doi:10.1126/science.209.4461.1116.

Gassó, S. (2008), Satellite observations of the impact of weak volcanic activity on marine clouds, *J. Geophys. Res.*, *113*, D14S19, doi:10.1029/2007JD009106.

Gauthier, P.-J., and M.-F. Le Cloarec (1998), Variability of alkali and heavy metal fluxes released by Mt. Etna volcano, Sicily, between 1991 and 1995, *J. Volcanol. Geotherm. Res.*, *81*(3–4), 311–326, doi:10.1016/S0377-0273(98)00002-X.

Gerlach, T. M. (2004), Volcanic sources of tropospheric ozone-depleting trace gases, *Geochem. Geophys. Geosyst.*, *5*, Q09007, doi:10.1029/2004GC000747.

Gerlach, T. M., H. Delgado, K. A. McGee, M. P. Doukas, J. J. Venegas, and L. Cárdenas (1997), Application of the LI-COR CO$_2$ analyzer to volcanic plumes: A case study, volcán Popocatépetl, Mexico, June 7 and 10, 1995, *J. Geophys. Res.*, *102*, 8005–8019, doi:10.1029/96JB03887.

Gerlach, T. M., K. A. McGee, A. J. Sutton, and T. Elias (1998), Rates of volcanic CO$_2$ degassing from airborne determinations of SO$_2$ emission rates and plume CO$_2$/SO$_2$: Test study at Pu'u'O'o Cone, Kilauea Volcano, Hawaii, *Geophys. Res. Lett.*, *25*, 2675–2678, doi:10.1029/98GL02030.

Graf, H.-F., J. Feichter, and B. Langmann (1997), Volcanic sulfur emission: Estimates of source strength and its contribution to the global sulfate distribution, *J. Geophys. Res.*, *102*, 10,727–10,738.

Hansell, A., and C. Oppenheimer (2004), Health hazards from volcanic gases: A systematic literature review, *Arch. Environ. Health*, *59*(12), 628–639, doi:10.1080/00039890409602947.

Hobbs, P. V., J. P. Tuell, D. A. Hegg, L. F. Radke, and M. W. Eltgrowth (1982), Particles and gases in the emissions from the 1980–1981 volcanic eruptions of Mt. St. Helens, *J. Geophys. Res.*, *87*, 11,062–11,086, doi:10.1029/JC087iC13p11062.

Hobbs, P. V., L. F. Radke, J. H. Lyons, R. J. Ferek, D. J. Coffman, and T. J. Casadevall (1991), Airborne measurements of particle and gas emissions from the 1990 volcanic eruptions of Mount Redoubt, *J. Geophys. Res.*, *96*, 18,735–18,752, doi:10.1029/91JD01635.

Hoppel, W. A., G. M. Frick, J. W. Fitzgerald, and B. J. Wattel (1994), A cloud chamber study of the effect that nonprecipitating water clouds have on the aerosol size distribution, *Aerosol Sci. Technol.*, *20*, 1–30, doi:10.1080/02786829408959660.

Horwell, C. J., and P. J. Baxter (2006), The respiratory health hazards of volcanic ash: A review for volcanic risk mitigation, *Bull. Volcanol.*, *69*(1), 1–24, doi:10.1007/s00445-006-0052-y.

Huey, L. G. (2007), Measurement of trace atmospheric species by chemical ionization mass spectrometry: Speciation of reactive nitrogen and future directions, *Mass Spectrom. Rev.*, *26*(2), 166–184, doi:10.1002/mas.20118.

Jacob, P., and D. Klockow (1992), Hydrogen peroxide measurements in the marine atmosphere, *J. Atmos. Chem.*, *15*, 353–360, doi:10.1007/BF00115404.

Jensen, E. J., and O. B. Toon (1992), The potential effects of volcanic aerosols on cirrus cloud microphysics, *Geophys. Res. Lett.*, *19*, 1759–1762, doi:10.1029/92GL01936.

Karagulian, F., L. Clarisse, C. Clerbaux, A. J. Prata, D. Hurtmans, and P. F. Coheur (2010), Detection of volcanic SO$_2$, ash, and H$_2$SO$_4$ using the Infrared Atmospheric Sounding Interferometer (IASI), *J. Geophys. Res.*, *115*, D00L02, doi:10.1029/2009JD012786.

Langmann, B., K. Zakšek, M. Hort, and S. Duggen (2010), Volcanic ash as fertiliser for the surface ocean, *Atmos. Chem. Phys.*, *10*, 3891–3899, doi:10.5194/acp-10-3891-2010.

Lawson, P. R., B. A. Baker, C. G. Schmitt, and T. L. Jensen (2001), An overview of microphysical properties of Arctic clouds observed in May and July 1998 during FIRE ACE, *J. Geophys. Res.*, *106*, 14,989–15,014, doi:10.1029/2000JD900789.

Lazrus, A. L., R. D. Cadle, B. W. Gandrud, J. P. Greenberg, B. J. Huebert, and W. I. Rose Jr. (1979), Sulfur and halogen chemistry of the stratosphere and of volcanic eruption plumes, *J. Geophys. Res.*, *84*, 7869–7875, doi:10.1029/JC084iC12p07869.

Lee, C., Y. J. Kim, H. Tanimoto, N. Bobrowski, U. Platt, T. Mori, K. Yamamoto, and C. S. Hong (2005), High ClO and ozone depletion observed in the plume of Sakurajima volcano, Japan, *Geophys. Res. Lett.*, *32*, L21809, doi:10.1029/2005GL023785.

Lelieveld, J., and P. J. Crutzen (1990), Influences of cloud photochemical processes on tropospheric ozone, *Nature*, *343*, 227–233, doi:10.1038/343227a0.

Longo, B. M., A. Grunder, R. Chuan, and A. Rossignol (2005), SO_2 and fine aerosol dispersion from the Kilauea plume, Kau district, Hawaii, USA, *Geology*, *33*(3), 217–220, doi:10.1130/G21167.1.

Mannino, D. M., S. Ruben, F. C. Holschuh, T. C. Holschuh, M. D. Wilson, and T. Holschuh (1996), Emergency department visits and hospitalizations for respiratory disease on the island of Hawaii, 1981 to 1991, *Hawaii Med. J.*, *55*(3), 48–54.

Martin, R. S., T. A. Mather, D. M. Pyle, M. Power, A. G. Allen, A. Aiuppa, C. J. Horwell, and E. P. W. Ward (2008), Composition-resolved size distributions of volcanic aerosols in the Mt. Etna plumes, *J. Geophys. Res.*, *113*, D17211, doi:10.1029/2007JD009648.

Martin, R. S., T. A. Mather, D. M. Pyle, M. Power, V. I. Tsanev, C. Oppenheimer, A. G. Allen, C. J. Horwell, and E. P. W. Ward (2009), Size distributions of fine silicate and other particles in Masaya's volcanic plume, *J. Geophys. Res.*, *114*, D09217, doi:10.1029/2008JD011211.

Martin, R. S., et al. (2010), A total volatile inventory for Masaya Volcano, Nicaragua, *J. Geophys. Res.*, *115*, B09215, doi:10.1029/2010JB007480.

Mather, T. A., D. M. Pyle, and C. Oppenheimer (2003a), Tropospheric volcanic aerosol, in *Volcanism and the Earth's Atmosphere, Geophys. Monogr. Ser.*, vol. 139, edited by A. Robock and C. Oppenheimer, pp. 189–212, AGU, Washington, D. C.

Mather, T. A., A. G. Allen, C. Oppenheimer, D. M. Pyle, and A. J. S. McGonigle (2003b), Size-resolved characterization of soluble ions in the particles in the tropospheric plume of Masaya volcano, Nicaragua: Origins and plume processing, *J. Atmos. Chem.*, *46*, 207–237, doi:10.1023/A:1026327502060.

Mather, T. A., V. I. Tsanev, D. M. Pyle, A. J. S. McGonigle, C. Oppenheimer, and A. G. Allen (2004a), Characterization and evolution of tropospheric plumes from Lascar and Villarrica volcanoes, Chile, *J. Geophys. Res.*, *109*, D21303, doi:10.1029/2004JD004934.

Mather, T. A., A. G. Allen, B. M. Davison, D. M. Pyle, C. Oppenheimer, and A. J. S. McGonigle (2004b), Nitric acid from volcanoes, *Earth Planet. Sci. Lett.*, *218*, 17–30, doi:10.1016/S0012-821X(03)00640-X.

McGee, K. A., M. P. Doukas, and T. M. Gerlach (2001), Quiescent hydrogen sulfide and carbon dioxide degassing from Mount Baker, Washington, *Geophys. Res. Lett.*, *28*, 4479–4482, doi:10.1029/2001GL013250.

McGonigle, A. J. S., P. Delmelle, C. Oppenheimer, V. I. Tsanev, T. Delfosse, G. Williams-Jones, K. Horton, and T. A. Mather (2004), SO_2 depletion in tropospheric volcanic plumes, *Geophys. Res. Lett.*, *31*, L13201, doi:10.1029/2004GL019990.

Möller, D. (1980), Kinetic model of atmospheric SO_2 oxidation based on published data, *Atmos. Environ.*, *14*, 1067–1076, doi:10.1016/0004-6981(80)90037-2.

Murphy, D. M., D. J. Cziczo, K. D. Froyd, P. K. Hudson, B. M. Matthew, A. M. Middlebrook, R. E. Peltier, A. Sullivan, D. S. Thomson, and R. J. Weber (2006), Single-particle mass spectrometry of tropospheric aerosol particles, *J. Geophys. Res.*, *111*, D23S32, doi:10.1029/2006JD007340.

Naoe, H., J. Heintzenberg, K. Okada, Y. Zaizen, K. Hayashi, T. Tateishi, Y. Igarashi, Y. Dokiya, and K. Kinoshita (2003), Composition and size distribution of submicrometer aerosol particles observed on Mt. Fuji in the volcanic plumes from Miyakejima, *Atmos. Environ.*, *37*, 3047–3055, doi:10.1016/S1352-2310(03)00295-4.

Oppenheimer, C., P. Francis, and J. Stix (1998), Depletion rates of sulfur dioxide in tropospheric volcanic plumes, *Geophys. Res. Lett.*, *25*, 2671–2674, doi:10.1029/98GL01988.

Oppenheimer, C., V. I. Tsanev, C. F. Braban, R. A. Cox, J. W. Adams, A. Aiuppa, N. Bobrowski, P. Delmelle, J. Barclay, and A. J. S. McGonigle (2006), BrO formation in volcanic plumes, *Geochim. Cosmochim. Acta*, *70*, 2935–2941, doi:10.1016/j.gca.2006.04.001.

Oppenheimer, C., et al. (2010), Atmospheric chemistry of an Antarctic volcanic plume, *J. Geophys. Res.*, *115*, D04303, doi:10.1029/2009JD011910.

Pearson, R. W., and D. H. Stedman (1980), Instrumentation for fast response ozone measurements from aircraft, *Atmos. Tech.*, *12*, 51–55.

Phelan Kotra, J., D. L. Finnegan, W. H. Zoller, M. A. Hart, and J. L. Moyers (1983), El Chichón: Composition of plume gases and particles, *Science*, *222*, 1018–1021, doi:10.1126/science.222.4627.1018.

Porter, J. N., and A. D. Clarke (1997), Aerosol size distribution models based on in situ measurements, *J. Geophys. Res.*, *102*, 6035–6045, doi:10.1029/96JD03403.

Porter, J. N., K. A. Horton, P. J. Mouginis-Mark, B. Lienert, S. K. Sharma, E. Lau, A. J. Sutton, T. Elias, and C. Oppenheimer (2002), Sun photometer and lidar measurements of the plume from the Hawaii Kilauea Volcano Pu'u O'o vent: Aerosol flux and SO_2 lifetime, *Geophys. Res. Lett.*, *29*(16), 1783, doi:10.1029/2002GL014744.

Radke, L. F., P. V. Hobbs, and J. L. Stith (1976), Airborne measurements of gases and aerosols from volcanic vents on Mt. Baker, *Geophys. Res. Lett.*, *3*, 93–96, doi:10.1029/GL003i002p00093.

Riley, C. M., W. I. Rose, and G. J. S. Bluth (2003), Quantitative shape measurements of distal volcanic ash, *J. Geophys. Res.*, *108*(B10), 2504, doi:10.1029/2001JB000818.

Roberts, T. J., C. F. Braban, R. S. Martin, C. Oppenheimer, J. W. Adams, R. A. Cox, R. L. Jones, and P. T. Griffiths (2009), Modelling reactive halogen formation and ozone depletion in volcanic plumes, *Chem. Geol.*, *263*, 151–163, doi:10.1016/j.chemgeo.2008.11.012.

Robock, A. (2000), Volcanic eruptions and climate, *Rev. Geophys.*, *38*(2), 191–219, doi:10.1029/1998RG000054.

Rodríguez, L. A., I. M. Watson, M. Edmonds, G. Ryan, V. Hards, C. M. M. Oppenheimer, and G. J. S. Bluth (2008), SO_2 loss rates in the plume emitted by Soufrière Hills volcano, Montserrat, *J. Volcanol. Geotherm. Res.*, *173*(1–2), 135–147, doi:10.1016/j.jvolgeores.2008.01.003.

Rose, W. I., R. L. Chuan, R. D. Cadle, and D. C. Woods (1980), Small particles in volcanic eruption clouds, *Am. J. Sci.*, *280*, 671–696, doi:10.2475/ajs.280.8.671.

Rose, W. I., et al. (2003), The February–March 2000 eruption of Hekla, Iceland from a satellite perspective, in *Volcanism and the Earth's Atmosphere, Geophys. Monogr. Ser.*, vol. 139, edited by A. Robock and C. Oppenheimer, pp. 107–132, AGU, Washington, D. C.

Rose, W. I., et al. (2006), Atmospheric chemistry of a 33–34 hour old volcanic cloud from Hekla volcano (Iceland): Insights from direct sampling and the application of chemical box modeling, *J. Geophys. Res.*, *111*, D20206, doi:10.1029/2005JD006872.

Sachse, G. W., G. F. Hill, L. O. Wade, and M. G. Perry (1987), Fast-response, high-precision carbon monoxide sensor using a tunable diode laser absorption technique, *J. Geophys. Res.*, *92*, 2071–2081, doi:10.1029/JD092iD02p02071.

Samaniego, P., J.-P. Eissen, J.-L. Le Pennec, C. Robin, M. L. Hall, P. Mothes, D. Chavrit, and J. Cotten (2008), Pre-eruptive physical conditions of El Reventador volcano (Ecuador) inferred from the petrology of the 2002 and 2004–05 eruptions, *J. Volcanol. Geotherm. Res.*, *176*(1), 82–93, doi:10.1016/j.jvolgeores.2008.03.004.

Sasano, Y., and E. V. Browell (1989), Light scattering characteristics of various aerosol types derived from multiple wavelength lidar observations, *Appl. Opt.*, *28*(9), 1670–1679.

Satsumabayashi, H., M. Kawamura, T. Katsuno, K. Futaki, K. Murano, G. R. Carmichael, M. Kajino, M. Horiguchi, and H. Ueda (2004), Effects of Miyake volcanic effluents on airborne particles and precipitation in central Japan, *J. Geophys. Res.*, *109*, D19202, doi:10.1029/2003JD004204.

Scheuer, E., R. W. Talbot, J. E. Dibb, G. K. Seid, L. DeBell, and B. Lefer (2003), Seasonal distributions of fine aerosol sulfate in the North American Arctic basin during TOPSE, *J. Geophys. Res.*, *108*(D4), 8370, doi:10.1029/2001JD001364.

Seinfeld, J. H., and S. N. Pandis (2006), *Atmospheric Chemistry and Physics: From Air Pollution to Climate Change*, 2nd ed., John Wiley, Hoboken, N. J.

Simkin, T., and L. Siebert (1994), *Volcanoes of the World*, 2nd ed., Geosci. Press, Tucson, Ariz.

Smith, D. B., R. A. Zielinski, W. I. Rose Jr., and B. J. Huebert (1982), Water-soluble material on aerosols collected within volcanic eruption clouds, *J. Geophys. Res.*, *87*, 4963–4972, doi:10.1029/JC087iC07p04963.

Smithsonian Institution (2008a), Tungurahua, *Bull. Global Volcanism Network*, *33*(6), 8–9.

Smithsonian Institution (2008b), Sangay, *Bull. Global Volcanism Network*, *33*(3), 15–16.

Spinei, E., S. A. Carn, N. A. Krotkov, G. H. Mount, K. Yang, and A. J. Krueger (2010), Validation of ozone monitoring instrument SO_2 measurements in the Okmok volcanic cloud over Pullman, WA, July 2008, *J. Geophys. Res.*, *115*, D00L08, doi:10.1029/2009JD013492.

Stith, J. L., P. V. Hobbs, and L. F. Radke (1978), Airborne particle and gas measurements in the emissions from six volcanoes, *J. Geophys. Res.*, *83*, 4009–4017, doi:10.1029/JC083iC08p04009.

Thompson, A. M. (1984), The effect of clouds on photolysis rates and ozone formation in the unpolluted troposphere, *J. Geophys. Res.*, *89*, 1341–1349, doi:10.1029/JD089iD01p01341.

Thornton, D. C., A. R. Bandy, B. W. Blomquist, D. D. Davis, and R. W. Talbot (1996), Sulfur dioxide as a source of condensation nuclei in the upper troposphere of the Pacific Ocean, *J. Geophys. Res.*, *101*, 1883–1890, doi:10.1029/95JD02273.

Toon, O. B., et al. (2010), Planning, implementation, and first results of the Tropical Composition, Cloud and Climate Coupling Experiment (TC[4]), *J. Geophys. Res.*, *115*, D00J04, doi:10.1029/2009JD013073.

Twohy, C. H., A. J. Schanot, and W. A. Cooper (1997), Measurements of condensed water content in liquid and ice clouds using an airborne counterflow virtual impactor, *J. Atmos. Oceanic Technol.*, *14*, 197–202, doi:10.1175/1520-0426(1997)014<0197:MOCWCI>2.0.CO;2.

Twomey, S. (1974), Pollution and the planetary albedo, *Atmos. Environ.*, *8*, 1251–1256, doi:10.1016/0004-6981(74)90004-3.

Vay, S. A., et al. (2003), The influence of regional-scale anthropogenic emissions on CO_2 distributions over the western North Pacific, *J. Geophys. Res.*, *108*(D20), 8801, doi:10.1029/2002JD003094.

von Glasow, R. (2010), Atmospheric chemistry in volcanic plumes, *Proc. Natl. Acad. Sci. U. S. A.*, *107*(15), 6594–6599, doi:10.1073/pnas.0913164107.

Wang, J., A. A. Hoffmann, R. Park, D. J. Jacob, and S. T. Martin (2008), Global distribution of solid and aqueous sulfate aerosols: Effect of the hysteresis of particle phase transitions, *J. Geophys. Res.*, *113*, D11206, doi:10.1029/2007JD009367.

Wang, Z., and K. Sassen (2000), Ozone destruction in continental stratus clouds: An aircraft case study, *J. Appl. Meteorol.*, *39*(6), 875–886, doi:10.1175/1520-0450(2000)039<0875:ODICSC>2.0.CO;2.

Watson, A. J. (1997), Volcanic iron, CO_2, ocean productivity and climate, *Nature*, *385*, 587–588, doi:10.1038/385587b0.

Wen, S., and W. I. Rose (1994), Retrieval of sizes and total masses of particles in volcanic clouds using AVHRR bands 4 and 5, *J. Geophys. Res.*, *99*, 5421–5431, doi:10.1029/93JD03340.

Wilson, L., and T. C. Huang (1979), The influence of shape on the atmospheric settling velocity of volcanic ash particles, *Earth Planet. Sci. Lett.*, *44*, 311–324, doi:10.1016/0012-821X(79)90179-1.

Yang, K., N. A. Krotkov, A. J. Krueger, S. A. Carn, P. K. Bhartia, and P. F. Levelt (2007), Retrieval of large volcanic SO_2 columns from the Aura Ozone Monitoring Instrument: Comparison and limitations, *J. Geophys. Res.*, *112*, D24S43, doi:10.1029/2007JD008825.

Yu, T., and W. I. Rose (2000), Retrieval of sulfate and silicate ash masses in young (1 to 4 days old) eruption clouds using multiband infrared HIRS/2 data, in *Remote Sensing of Active Volcanism*, *Geophys. Monogr. Ser.*, vol. 116, edited by P. J. Mouginis-Mark, J. A. Crisp, and J. H. Fink, pp. 87–100, AGU, Washington, D. C.

B. E. Anderson, E. V. Browell, G. Diskin, J. W. Hair, G. Sachse, and S. A. Vay, Science Directorate, NASA Langley Research Center, Hampton, VA 23681, USA.

S. A. Carn, Department of Geological and Mining Engineering and Sciences, Michigan Technological University, Houghton, MI 49931, USA. (scarn@mtu.edu)

J. Crounse, K. Spencer, and P. Wennberg, Department of Geological and Planetary Sciences, California Institute of Technology, Pasadena, CA 91125, USA.

J. E. Dibb, Department of Earth Sciences, University of New Hampshire, Durham, NH 03824, USA.

K. D. Froyd, NOAA Earth System Research Laboratory, Boulder, CO 80305, USA.

N. A. Krotkov, Goddard Earth Sciences and Technology Center, University of Maryland Baltimore County, Baltimore, MD 21228, USA.